Investigation of T Cell Chemotaxis and Electrotaxis Using Microfluidic Devices

by

Jing Li

A Thesis submitted to the Faculty of Graduate Studies of

The University of Manitoba

in partial fulfillment of the requirements of the degree of

MASTER OF SCIENCE

Department of Physics and Astronomy

University of Manitoba

Winnipeg, MB, Canada

Abstract

Directed immune cell migration plays important roles in immunosurveillance and immune responses. Understanding the mechanisms of immune cell migration is important for immune cell trafficking mediated physiological processes and diseases. Immune cell migration can be directed by various guiding cues such as chemical gradients and direct current electric fields (dcEF). Microfluidic devices have been increasingly developed for cell migration studies. These devices can precisely configure and manipulate chemical gradients and dcEF, and thus provide quantitative test beds for studying the complex guiding mechanisms for cell migration. In this thesis, two microfluidic devices were developed for producing controlled dcEF and used to analyze electrotaxis of activated T cells. Furthermore, a novel microfluidic device was developed to configure single or co-existing chemical gradients and dcEF to mimic the complex guiding environments in tissues and it was used to investigate the competition of chemical gradients and dcEF in directing T cell migration.

Acknowledgements

First and foremost, I would like to thank Dr. Francis Lin, my advisor, for his generous help and support. He always helps me with helpful suggestions and ideas to overcome the problems that I encountered during my research and study. It is my great pleasure to work with him.

I thank Dr. Can-Ming Hu and Dr. Arkady Major, my committee members, for their efforts to evaluate this work.

I also thank our current lab members: Saravanan Nandagopal, Jiandong Wu, Xun Wu, Kanmani Natarajan and Dr. Dan Wu for their support and assistance. Especially thanks to Saravanan Nandagopal for teaching me basic biological skills and knowledge initially. I would also like to thank our previous lab members Dr. Ling Zhu for helping with cell migration data analysis and Nitin Wadhawan for collaborating on developing and testing new microfluidic devices.

I thank Dr. Douglas Thomson and Mr. Sean Romanuik from Department of Electrical and Computer Engineering for helping with the COMSOL simulations of our microfluidic devices.

I thank Mr. Dwayne Chrusch from Nano Systems Fabrication Laboratory (NSFL) for helping me with the device fabrication, Ms. Shauna Leeson from The Victoria General Hospital (VGH) in Winnipeg for helping obtaining blood samples, Dr. Kennedy Makondo for helping with flow cytometry and James Dietrich for helping with the microfluidic glass device assembly.

Great thanks to Manitoba Health Research Council (MHRC) for the Graduate Student Fellowship, Faculty of Science of the University of Manitoba for the Faculty of Science Scholarship and my home department (Department of Physics and Astronomy) for the excellent support to my graduate study.

I would like to acknowledge the products, services and financial support for the device fabrication provided by CMC Microsystems (www.cmc.ca) that facilitated this research.

Last but not least, I would like to thank my wonderful parents and friends for their continual support.

Table of Contents

Abstract……..……...……...2

Acknowledgements……..……...…..3

Table of Contents……...……...…….5

List of Figures……...……...……...9

List of Tables..……..…….....11

List of Abbreviations……..……..……12

Chapter 1: Introduction……..……..……...13

1.1 Directed cell migration……..……..……13

1.2 Chemotaxis, conventional assays and microfluidic devices……..……..13

1.3 Electrotaxis, conventional assays and microfluidic devices……..……..14

1.4 Motivation for the research in this thesis……..……...19

Chapter 2: Cell Migration……..…….20

2.1 Cell migration……..……20

2.2 Chemotaxis and immune cell trafficking…….20

2.3 Electrotaxis……..……23

Chapter 3: Conventional chemotaxis assays and microfluidic devices……...26

3.1 Conventional chemotaxis assays……..26

3.1.1 Boyden chamber/transwell assay……..26

3.1.2 Zigmond chamber and Dunn chamber…….28

3.1.3 Under-agarose assay……....….28

3.1.4 Micropipette-based assay……..28

3.2 Flow-based microfluidic devices…….28

3.3 Flow-free microfluidic devices……...29

Chapter 4: Conventional electrotaxis assays and microfluidic devices……...33

4.1 Electrotaxis and conventional assays……...33

4.2 Microfluidic devices……34

Chapter 5: General methodologies……...39

5.1 Microfluidic device preparation……...39

5.1.1 Device design……39

5.1.2 Photolithography……...39

5.1.3 Soft-lithography……39

5.1.4 Fabrication procedures of microfluidic devices……40

5.2 Cell preparation……43

5.3 Experimental setup……...45

5.4 Data analysis……45

5.5 COMSOL multiphysics modeling……...48

Chapter 6: T cell migration in specific microfluidic chemotaxis and electrotaxis devices……49

6.1 Introduction……..49

6.2 Methodology……49

6.2.1 Cell preparation……50

6.2.2 Microfluidic device preparation……50

6.2.2.1 PDMS electrotaxis and chemotaxis devices……..50

6.2.2.2 Glass electrotaxis device……53

6.2.3 Cell migration experiment……55

6.2.4 Data analysis……58

6.3 Results……58

6.3.1 Electrotaxis and chemotaxis of activated T cells in PDMS microfluidic device……58

6.3.2 Electrotaxis of activated T cells in glass microfluidic device with integrated electrodes…67

6.4 Discussion and conclusion……...69

Chapter 7: T cell migration in co-existing chemical gradients and DC electric fields in microfluidic devices……...73

7.1 Introduction……..73

7.2 Methodology……75

7.2.1 Cell preparation……75

7.2.2 Microfluidic device preparation……75

7.2.3 Multiphysics modeling……..78

7.2.4 Cell migration experiment setup……...78

7.2.5 Data analysis……79

7.3 Results……..79

7.3.1 Generation of controlled chemical gradients and dcEF using the microfluidic device……79

7.3.2 T cell chemotaxis to single chemokine gradients in the microfluidic device……...85

7.3.3 T cell electrotaxis to single dcEF in the microfluidic device……87

7.3.4 T cell migration in competing chemokine gradient and dcEF in the microfluidic device…90

7.4 Discussion and conclusion……...93

Chapter 8: Conclusion remarks and outlook……..99

References……102

Publications……...……...……111

List of Figures

Fig 1-1. Illustration of microfluidic devices for chemotaxis and electrotaxis studies……...17

Fig 1-2. Illustration of petri dish based electrotaxis assay……...18

Fig 1-3.Leukocyte trafficking to target sites in tissues…….....22

Fig 2-2. Illustration of possible mechanisms for cell migration in response to chemical gradients and electric fields……25

Fig 3-1. Illustration of Boyden chamber……27

Fig 5-1. Illustration of photolithography……...42

Fig 5-2. Illustration of cell preparation……..44

Fig 5-3. Illustration of microfluidic cell migration data analysis……47

Fig 6-1. Illustration of the PDMS microfluidic electrotaxis device…….51

Fig 6-2. Illustration of the "Y" shape microfluidic chemotaxis device……...52

Fig 6-3. Illustration of the glass microfluidic electrotaxis device…….....54

Fig 6-4. Cell migration experimental setup……...57

Fig 6-5. Simulation of dcEF in the PDMS microfluidic electrotaxis device……...60

Fig 6-6. Simulation of dcEF in the glass microfluidic electrotaxis device……..61

Fig 6-7. Electrotaxis of activated T cell in microfluidic devices……..62

Fig 6-8. T cell migration in chemical gradients and dcEF in the PDMS microfluidic devices

……65

Fig 6-9. T cell chemotaxis in the PDMS microfluidic device……...66

Fig 7-1. Schematic illustration of the microfluidic device……...77

Fig 7-2. Simulation of dcEF in the microfluidic device……..81

Fig 7-3. Simulation of chemical concentration gradients with dcEF application in the microfluidic device……..84

Fig 7-4. T cell chemotaxis in the microfluidic device……86

Fig 7-5. T cell electrotaxis in the microfluidic device……88

Fig 7-6. T cell migration in competing CCL19 gradients and dcEF in the microfluidic device……91

List of Tables

Table 3-1. Microfluidic chemotaxis devices……...31

Table 4-1. Microfluidic electrotaxis devices……..38

Table 6-1. Quantitative comparison of chemotaxis and electrotaxis of activated T cells in microfluidic devices…….68

List of Abbreviations

dcEF: direct current electric fields

TEP: transepithelial potentials

DC: direct current

2D: two-dimensional

3D: three-dimensional

ECM: extracellular matrix

EGFR: epidermal growth factor receptors

O.I.: orientation index

M.I.: motility index

S.E.M.: standard error of mean

PDMS: polydimethylsiloxane

PBS: Phosphate buffered saline

BSA: Bovine serum albumin

Chapter 1

Introduction

1.1 Directed cell migration

Directed cell migration is involved in a broad range of physiological and pathological processes such as embryogenesis, inflammatory responses, wound healing and cancer metastasis [1-8]. For example, white blood cells such as neutrophils and lymphocytes can detect and follow gradients of tissue-derived chemical factors (i.e. chemoattractants) to perform their immune functions [1]. Misdirected white blood cells can cause various diseases and disorders such as chronic obstructive pulmonary disease (COPD), inflammatory bowel disease (IBD) and multiple sclerosis (MS) [1, 9]. Directed cell migration is a highly ordered process largely orchestrated by diverse cellular guiding signals [10, 11]. Here we focus on discussing the chemical and electrical guiding mechanisms and relevant cell migration assays and microfluidic devices.

1.2. Chemotaxis, conventional assays and microfluidic devices

Chemotaxis is a process that cells and other organisms migrate in response to soluble chemical concentration gradients. In addition to immune cells, many other cell types are capable of chemotactic migration in physiological processes. For example, tumor cells migrate toward gradients of various tissue-derived chemoattractants (e.g. epidermal growth factor, stromal cell-derived factor) resulting in more severe metastases [2, 12, 13]. Other examples include epithelial cell migration in wound healing and neural crest cell migration in embryo development [6, 14].

Because of the high biological and physiological relevance of chemotaxis, understanding its mechanisms has been a long-time focus in cell migration research. Historically, various

conventional assays (e.g. the transwell assay or Boyden chamber, under-agarose assay, micropipette-based assay, Zigmond chamber and Dunn chamber that produce chemical concentration gradients by free diffusion) [15-19] have been widely used for cell migration experiments. These assays typically lack the ability to maintain and control chemical gradients and some do not allow real-time quantification of cell migration at the single-cell level. Recently, microfluidic devices, which are microfabricated chips consisting of channels with micrometer dimensions (Fig. 1-1), have been increasingly applied to chemotaxis studies. Microfluidic devices allow well-defined and stable chemical concentration gradients and offer many advantages in terms of miniaturization, low reagent consumption and the potential for high-throughput experimentation [20]. In particular, microfluidic devices allow more efficient and quantitative evaluations of cell migration in spatiotemporally complex chemoattractant fields that better mimic *in-vivo* situations [20]. As an example, microfluidic devices have significantly advanced our understanding of neutrophils to adapt to and integrate complex chemical guiding signals for robust and effective chemotactic navigation [21, 22].

Chemical gradient guided cell migration and these relevant conventional assays and microfluidic devices will be discussed in more details in later chapters.

1.3 Electrotaxis, conventional assays and microfluidic devices

In addition to chemical gradients, physiological or externally applied direct current electric fields (dcEF) can also serve as a guiding mechanism for the orientation and movement of many cell types, such as epithelial cells, endothelial cells, cancer cells, fission yeast cells, leukocytes and *Dictyostelium*. When cells move in response to an electric field, it is commonly referred as electrotaxis or galvanotaxis. A well-known example is epithelial cell electrotaxis for wound

healing: the wound causes disruption of epithelial barrier and short-circuits the transepithelial potentials (TEP) at the wound, thus produces an electric field with the wound as the cathode, which attracts the surrounding epithelial cells. The sensing mechanisms of electrical signals by the cells are not clear although some studies have suggested that electromigration of some cell surface receptors and some ion channels in cells may be involved. In addition to epithelial cells, many cell types also migrate toward the cathode (e.g. neural crest cells, fibroblasts, keratinocytes, rat prostate cancer cells, mouse neutrophils, human myeloid cell lines, human peripheral blood T cells) while other cells migrate toward the anode (e.g. corneal endothelial cells, and human vascular endothelial cells) of an externally applied electric field in *in-vitro* experiments. However, in contrast to the more matured field of chemotaxis, the mechanism of electrotaxis is not well defined.

As a relatively new research area compared to chemotaxis, electrotaxis has recently attracted growing interest from a broad range of scientists aiming to explore its physiological applications and underlying mechanisms [6]. Petri dish-based assay is the most commonly used assay for studying electrotaxis. In this assay, a cell culture chamber is located in the center of a Petri dish, the rest part of the Petri dish is filled with cell migration medium, and the DC electric field is applied to the cell culture chamber through a pair of agar salt bridges [3, 23-27] (Fig. 1-2). Despite their wide use, the Petri dish-based assays have limitations including difficulty in controlling the electric field, low experimental throughput, and lack of miniaturization.

Recently, microfluidic devices have been used to identify and investigate electrotaxis of different cell types in a number of studies [28], suggesting a growing trend of integrating microfluidics with electrotaxis research [29-31]. In microfluidic devices, uniform electric fields are applied to

cells seeded in microfluidic channels, enabling real-time visualization and quantitative electrotaxis analysis at the single cell level. Furthermore, miniaturization of microfluidic devices reduces the Joule heating effect [28] and allows high-throughput experiments to be conducted on a single chip.

DC electric field guided cell migration and these relevant conventional assays and microfluidic devices will be discussed in more detail in later chapters.

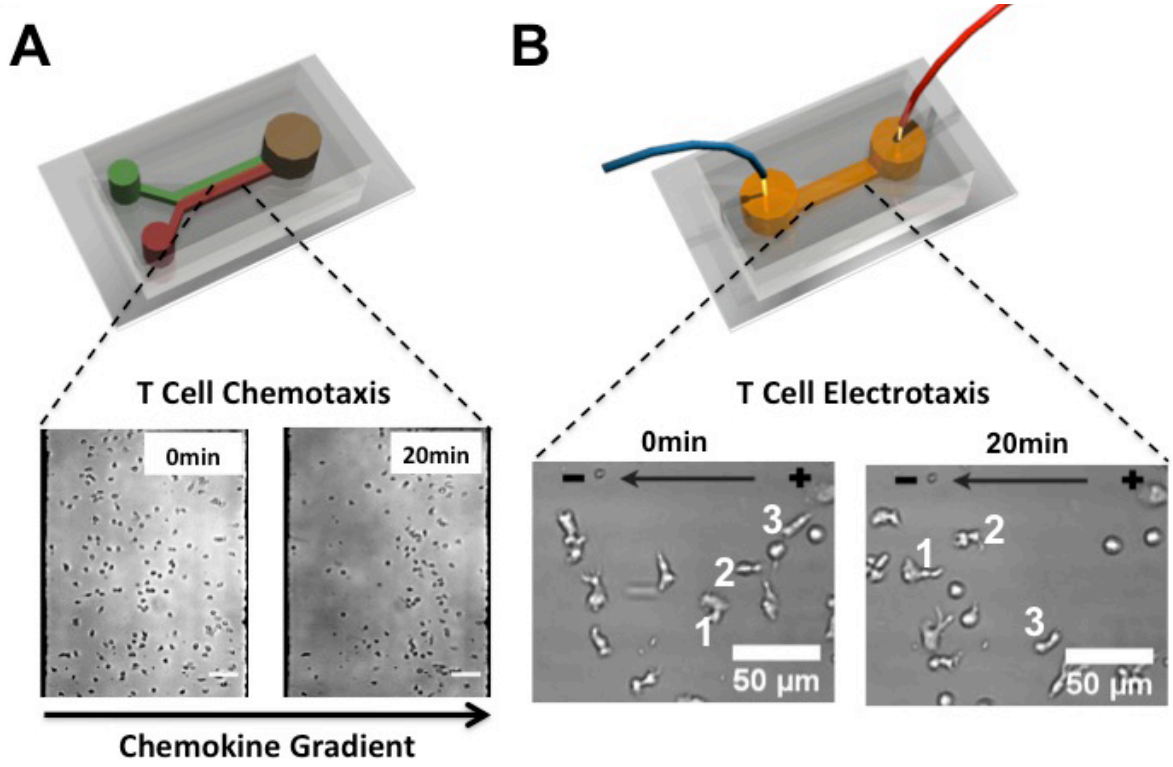

Fig 1-1. Illustration of microfluidic devices for chemotaxis and electrotaxis studies. *(A) Illustration of the simple "Y"-type PDMS microfluidic device for generating chemical concentration gradients based on continuous laminar flow mixing. The bottom figures show human T cell chemotaxis to a chemokine CCL19 gradient in the "Y"-type device. The scale bar represents 50 μm [32]. (B) Illustration of the PDMS microfluidic electrotaxis device. The DC electric field is applied to the straight microfluidic channel through the external electrodes inserted into the medium reservoirs at the ends of the channel. The bottom figures show human T cell electrotaxis toward the cathode of the applied electric field in the microfluidic device. The scale bar represents 50 μm [33]. Reproduced with permission from Elsevier.*

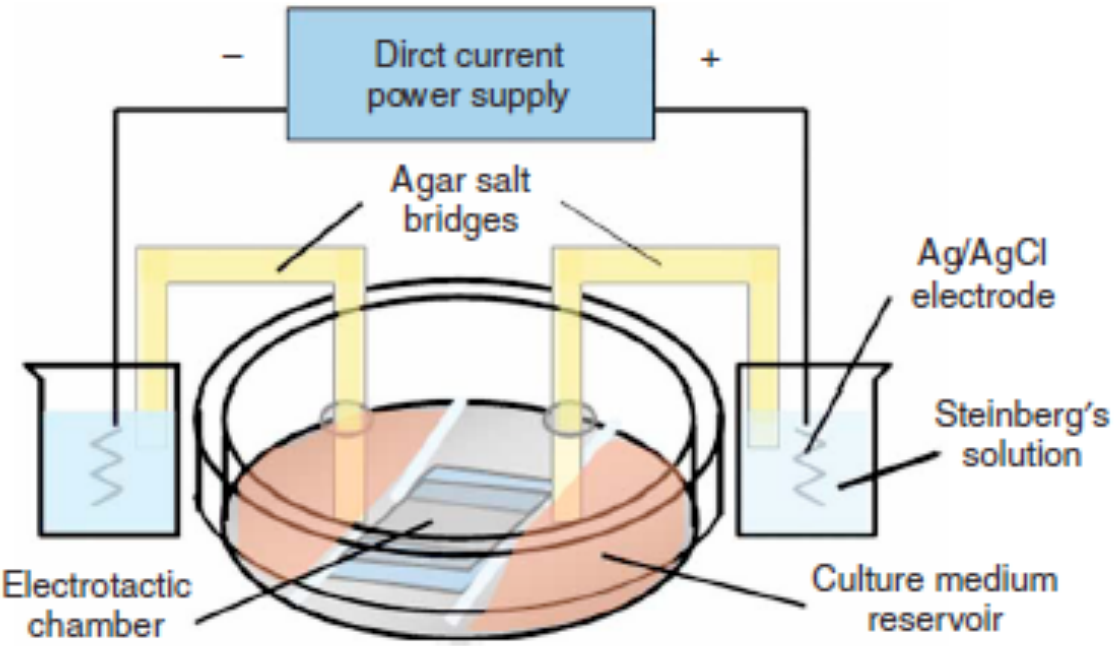

Fig 1-2. Illustration of petri dish based electrotaxis assay. *A cell culture chamber is located in the center of a Petri dish, the rest part of the Petri dish is filled with cell migration medium, and the DC electric field is applied to the cell culture chamber through a pair of agar salt bridges [25]. Reproduced with permission from Nature Publishing Group.*

1.4 Motivation for the research in this thesis

Given the importance of chemical gradient- and electric field-directed cell migration and the suitability of microfluidic devices for cell migration studies in better controlled cellular environments, we are motivated to develop microfluidic devices for quantitative characterizations of cell chemotaxis and electrotaxis. Specifically, we focused on characterizing and comparing chemotaxis and electrotaxis of activated human peripheral blood T cells in a consistent microfluidic platform. Furthermore, because multiple chemical gradients as well as electric fields can potentially co-exist in tissues, the interplay of these different cues in directing cell migration and movement (e.g. co-existing chemical gradients and electric fields for mediating epithelial cell migration in wound healing) needs to be better understood. Microfluidic devices have the potential to configure such complex chemical and electric fields in a highly controlled manner. Therefore, we are also motivated to develop new microfluidic systems that can configure better controlled co-existing chemical gradients and electric fields to study the competition of the chemical and electrical signals in guiding T cell migration.

Following the general background information introduced in this chapter, the rest of the thesis is organized by first reviewing chemical and electrical guiding mechanisms for cell migration (Chapter 2) and relevant conventional cell migration assays and microfluidic devices for chemotaxis and electrotaxis (Chapter 3 and 4), and subsequently describing the methodologies and results of my research (Chapter 5-7), and ending by discussing potential future directions (Chapter 8).

Chapter 2

Cell Migration

2.1 Cell migration

Cell migration is fundamental to cell and tissue dynamics in wound healing, cancer metastasis, immune responses as well as embryogenesis [1-4]. Cell migration can be roughly divided into two categories: migration through medium such as bacterial swimming and migration through a two-dimensional (2D) or three-dimensional (3D) solid extracellular matrix (ECM) [34]. The biological mechanisms of directed cell locomotion are complex and depend on the mode of cell locomotion and the cell type [11, 34]. For mammalian cells, they migrate within solid ECM via a cyclical process involving complex signal transduction, cytoskeleton reorganization and cell-ECM interactions [35].

2.2 Chemotaxis and immune cell trafficking

Chemical concentration gradient is one of the most important guiding cues for directing cell migration. For mammalian cells, they can detect minute concentration difference of chemical factors (i.e. chemoattractants) across the cell body and adjust their migration toward the chemoattractant gradients (i.e. chemotaxis). The chemical gradient is sensed through specific cell surface receptors that subsequently trigger complex downstream signal cascades leading to directed cell migration. Phosphatidylinositide-3 kinases (PI3Ks), phosphatase tensin homolog on chromosome 10 (PTEN), PtdIns(3,4,5)P3 (PIP3), PtdIns(3,4)P2 (PI(3,4)P2) and Cdc42 are some of the key downstream signaling molecules for gradient sensing and migration for many cell types.

Such a chemical-based guiding mechanism is important for immune cell trafficking tissues. Briefly, the recruitment of immune cells to the sites of inflammation is a combinatorial process that consists a sequence of tightly regulated cellular events including cell adhesion to endothelium followed by extravasation into tissues and chemotaxis in tissues to the target sites directed by specific chemoattractant gradients [36] [37] (Fig 2-1).

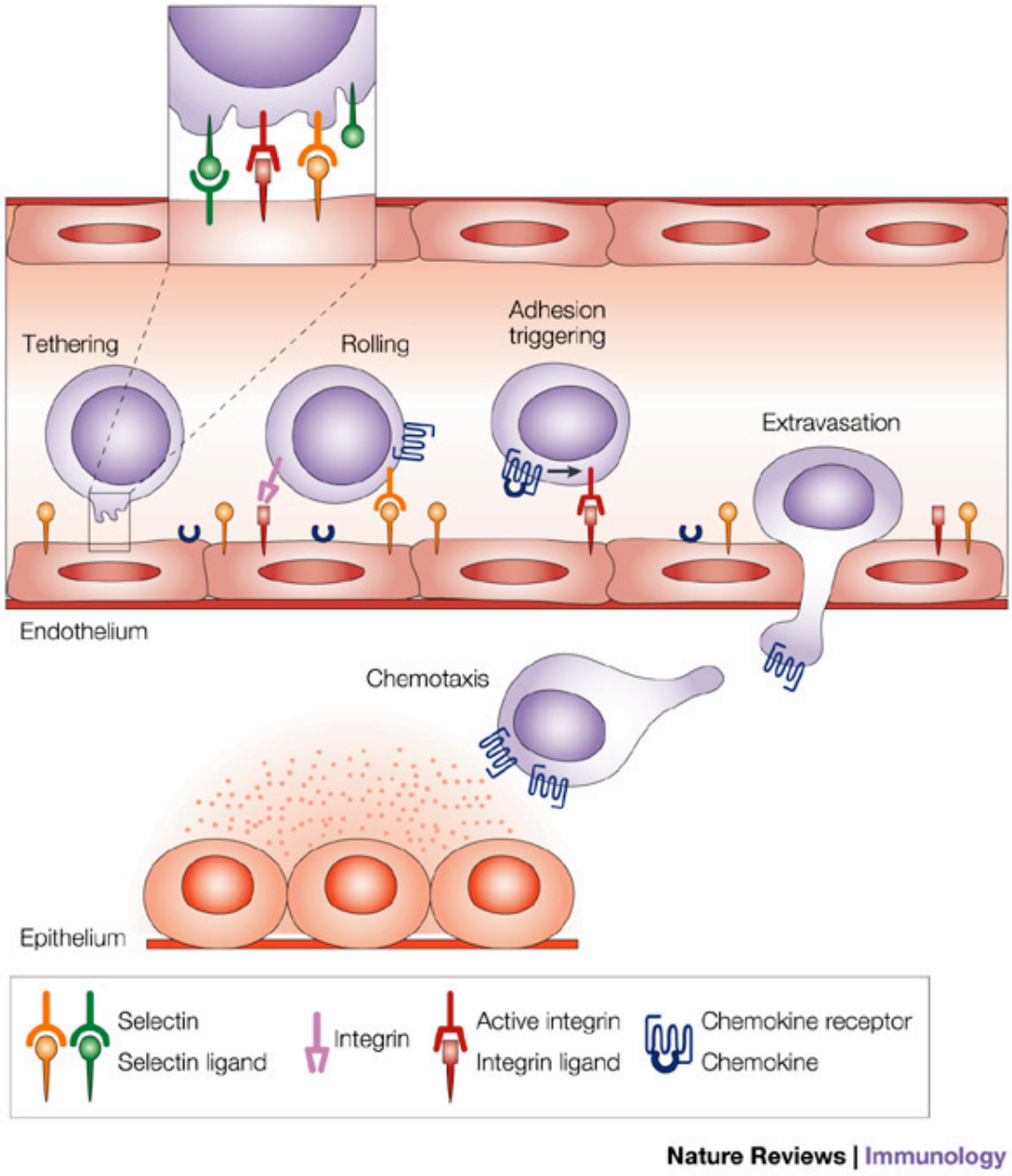

Fig 2-1. Leukocyte trafficking to target sites in tissues. *A multi-step process including tethering, rolling, adhesion, extravasation and chemotaxis [36]. Reproduced with permission from Nature Publishing Group.*

2.3 Electrotaxis

As a relatively new research area compared to chemotaxis, electrotaxis has recently attracted growing interest from a broad range of scientists aiming to explore its physiological applications and underlying mechanisms. Previous studies have shown that phosphatidylinositol-3-OH kinase-g [PI(3)Kg] and the phosphatase and tensin homolog (PTEN) are important for both chemotactic and electrotactic signaling in different cell types [3, 38-42]. In addition, it has been shown that ion channels such as Ca^{2+} and Na^{+} channels and the associated downstream cellular signaling are required for electrotaxis [24, 43-45]. Interestingly, human granulocytes move towards the anode of the electric field in medium containing 2.5 mM Ca^{2+}, but move towards the cathode in medium with a lower Ca^{2+} content (0.1 mM) [46]. The mechanism of this Ca^{2+}-dependent bi-directional electrotactic response of granulocytes is not clear, however. More strikingly, the direction of electrotactic movement of *Dictyostelium* can be reversed by genetic modulation of specific signaling molecules that mediate cathode-directing or anode- directing electrotaxis of cells, as shown by an *in vitro* experimental study [47]. Although this field is still emerging, evidence suggests that electrotactic sensing and the resulting migration or movement is a highly complex process, dependent on cell type, medium conditions, and diverse intracellular signaling cascades. Extensive further research is needed to elucidate the physiological mechanisms for electrotaxis in different cell types and organisms [28] (Fig. 2-2). Particularly, previous studies have demonstrated the cathode-directing electrotaxis of human peripheral blood memory T cells [29] that motivated us to further investigate electrotaxis of other T cell types.

More importantly, it is expected that physiological chemical gradients and DC electric fields can potentially co-exist in tissues and the two guiding mechanisms may direct cell migration in a

coordinated manner. Fig. 2-2 shows the possible mechanisms for cell migration in response to chemical gradients and DC electric fields. Briefly, cells are exposed to tissue-produced chemoattractant gradients with complex profiles in space and time, and can also be subject to electric fields, such as occur at wound sites. Cells can migrate along chemoattractant gradients through specific chemoattractant receptor signaling. Several mechanisms for electric field guided cell migration have also been suggested such as electromigration of cell surface receptors [14] and calcium signaling [43]. Clarification of the mechanisms for electrotaxis and the interplay between electrotaxis and chemotaxis will aid in understanding the outcomes of directional decision making in cell orientation and migration in co-existing chemical gradients and electric fields. Such studies require innovations in developing sophisticated experimental methods to allow quantitative analysis of cell migration in controlled simple or complex chemical and electrical guiding environments.

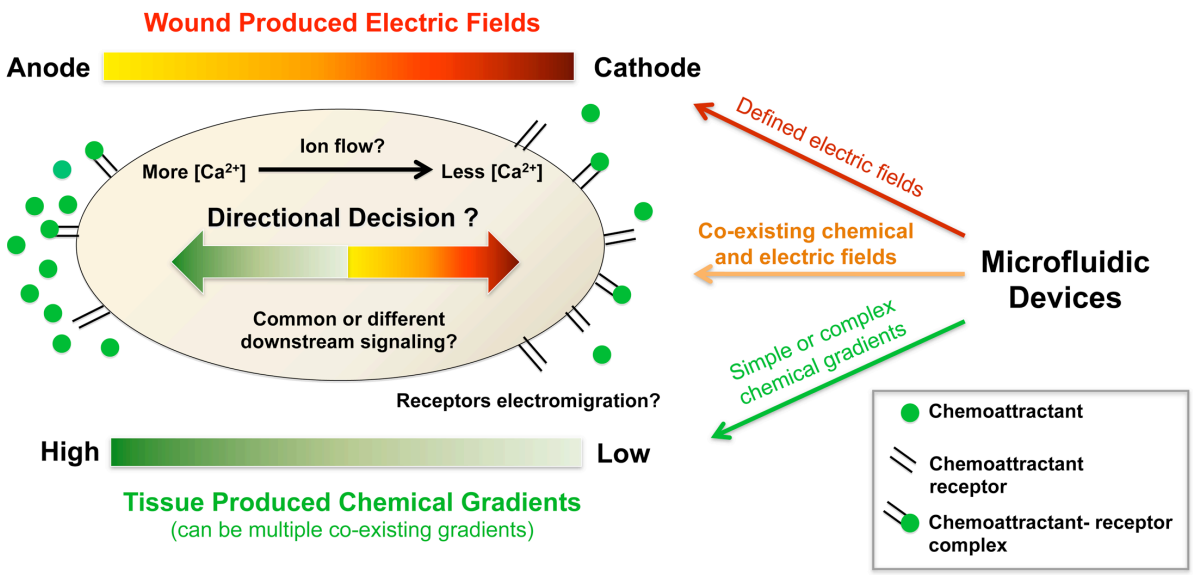

Fig 2-2. Illustration of possible mechanisms for cell migration in response to chemical gradients and electric fields [28]. *Reproduced with permission from Elsevier.*

Chapter 3

Conventional chemotaxis assays and microfluidic devices

3.1 Conventional chemotaxis assays

3.1.1 Boyden chamber/transwell assay

Historically, several conventional cell migration assays have been used for chemotaxis studies. Boyden chamber/transwell assays is one of the most commonly used assays for studying cell migration and chemotaxis [15]. The chamber contains two compartments that are separated by filter membranes. Chemoattractants diffuse from the bottom compartment to the upper compartment through the membrane generating a gradient (Fig. 3-1) [48]. Cells are initially loaded to the upper compartment and the migrated cells to the bottom compartment through the membrane in responses to the chemoattractant gradient are counted at the end of the experiment. This assay requires large amount of input cells and does not allow visualization of cell movement.

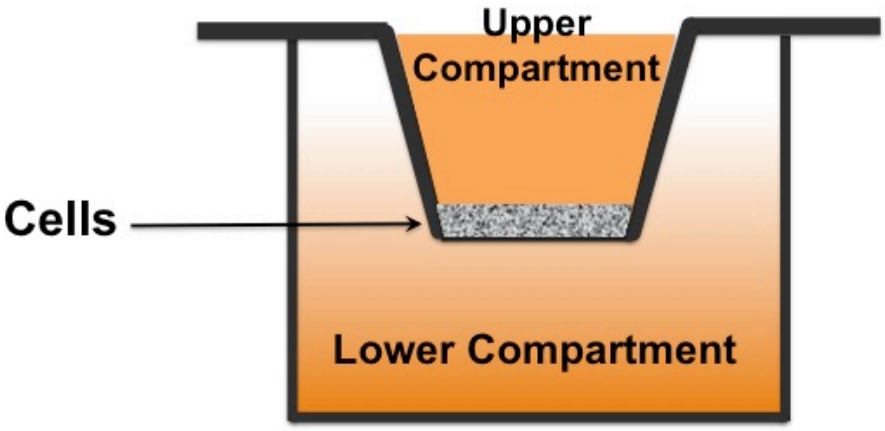

Fig 3-1. Illustration of Boyden chamber. *Two compartments are separated with a porous membrane in which cells can migrate through. The chemoattractant solution is filled in the lower compartment creating a gradient across the membrane by free diffusion. Cells are allowed to migrate from the upper compartment to the lower compartment through the membrane.*

3.1.2 Zigmond chamber and Dunn chamber

The Zigmond chamber [16] and its variant, namely the Dunn chamber [18], allow direct observation of chemotaxis in gradients. Such chambers consist of a plexiglass slide containing two wells separated by a bridge. A coverslip with cells attached is invertly placed over the bridge and wells, and the wells are filled with different concentrations of chemoattractants. The concentration gradient develops over the bridge by diffusion of chemoattractants. Cells migration in the gradient can be visualized under a microscope.

3.1.3 Under-agarose assay

The under-agarose chamber consists of a piece of agarose gel cast on a glass coverslip; wells for cells and test substance are punched into the agarose gel [19, 48] (Fig. 3-2). The chemical gradient develops by the diffusion of the chemoattractant through the gel and cell migration in response to the gradient can be quantified at both the population level and single cell level. This assay has the unique ability to configure multiple superimposed chemical gradients in 2D.

3.1.4 Micropipette-based assay

The micropipette-based assay releases chemoattractants from a pipette tip to the cell region in a medium reservoir and single cell movement can be observed directly [17]. The unique advantage of this assay is the ability to move the pipette and observe the cell as it reorients towards the source of chemoattractants. This assay allows direct visualization of cell motion in dynamic and superimposed chemical gradient environments.

While these single cell based assays are useful for cell migration and chemotaxis studies, their common limitation is the lacking of gradient condition controls.

3.2 Flow-based microfluidic devices

Conventional chemotaxis assays produce poorly controlled chemical gradients based on free diffusion and often require large amounts of reagents and cell samples, whereas microfluidic devices offer new experimental platforms for quantitative cell migration studies in better controlled gradient environments with reduced requirements for reagents and cells [20, 49]. Microfluidic gradient devices can be categorized as either flow-based devices or flow-free devices (Table 3-1). The flow-based microfluidic devices produce relatively long-range stable gradients by controlling the mixing of laminar flows of different chemicals or different concentrations of the same chemical in the microfluidic channels [20, 32, 50, 51] (Fig. 1-2). These microfluidic devices allow precise configurations of stable gradients with simple or complex shapes and flexible manipulations of gradients in space and time that mimic the multiple and dynamically varying chemoattractant gradients seen *in vivo* such as co-existing and time-evolving chemoattractant gradients for directing leukocyte trafficking in tissues. The flow-based devices have been broadly used for studying chemotaxis in different cell types, such as bacteria, neutrophils, cancer cells, lymphocytes and dendritic cells [32, 52-55] (Fig. 1-1). The migration and movement of cells had also been investigated in more complex and physiologically relevant gradient environments were also investigated, such as single gradients with different shapes (linear or nonlinear gradients that correspond to different stage of the diffusion process of the chemoattractant molecules), co-existing competing gradients, or fast temporally varying gradients [32, 50-52, 55]. Such studies would be difficult to perform using conventional assays.

3.3 Flow-free microfluidic devices

In contrast to the flow-based devices, flow-free microfluidic devices minimize the flow effect

such as flow induced shear stress on cell migration and movement, and allow higher throughput of experimentation with improved portability resulting from a reduced requirement for external controls, and also permit studies of cell-cell interactions in defined static gradient environments [56-59]. In particular, the advantages of the flow-free devices in experiment throughput and portability would allow more efficient cell migration measurements in a common life science lab setting. On the other hand, the ability to manipulate gradients is reduced in flow-free devices. Some representative strategies include membrane-based devices, microinjection and 3D gel devices, and these have been applied to the study of the migration and chemotaxis of different cell types, such as immune cells and cancer cells in 2D and 3D environments that mimic the ECM in tissues [58-60]. In a very interesting recent study, a microfluidic device consisting of bifurcating gradient channels of different paths to the chemoattractant source was used to test directional chemotactic decision-making by neutrophils [61]. The results show that cells preferentially migrate toward the chemoattractant gradient via the shorter path resulting from the stronger spatiotemporal chemotactic attraction from the short path. As uniquely revealed by this microfluidics-based experiment, neutrophils are capable of making smart and economic decisions for effective and efficient directional migration in a “confusing” gradient environment [61]. These results also open up the question if similar mechanisms apply to other cell types that can be examined using similar microfluidics-based methods.

Table 3-1. Microfluidic chemotaxis devices

In general, microfluidic gradient devices can be categorized into two major classes.

1. The first class of microfluidic devices produces stable gradients based on controlled mixing of laminar flows of different chemicals. Mixing of laminar flows across the microfluidic channel width can be precisely controlled that allows precise configurations of stable chemical concentration gradients across the channel and the gradient profile is relatively stable over a long distance along the channel. By integrating multiple such gradients — generating modules in parallel and adjusting the configurations and relative flow rates of chemical inputs — complex gradient shapes, multiple co-existing gradients and dynamic gradients can be flexibly configured. The devices are typically coated with cell seeding and migration substrates and cell migration is visualized and recorded by time-lapse microscopy.

2. The second class of microfluidic devices generates time-evolving or stable chemical gradients in a flow-free environment. These devices use large chemical reservoirs or continuous chemical flows and allow chemicals to mix by free diffusion in microfluidic channels. Because of the small dimensions of microfluidic mixing channels compared to the volume of the chemical sources, the development of the gradient over time can be controlled and a stable gradient can be established at the equilibrium state of diffusion. Different channel depths for the chemical reservoirs and mixing channels, controlled chemical injection, use of membranes between different chemical reservoirs and the mixing channels, and introduction of gel structures to the channels are commonly used strategies to control chemical delivery and mixing and thus the 2D and 3D gradient formation in flow-free devices. The 3D gradients in gels better mimic tissue environments

and thus are more physiologically relevant for certain cell types. Like in flow-based devices, labeled (e.g. transfected to express GFP) or non-labeled cells are seeded in the gradient channel and cell migration is visualized and recorded by time-lapse microscopy.

Chapter 4

Conventional electrotaxis assays and microfluidic devices

4.1 Electrotaxis and conventional assays

Endogenous direct-current (DC) electric fields widely exist in biological systems [14, 43, 62] and play significant roles in a number of biological processes including tissue regeneration, embryo development, cell division, and nerve growth [14, 63-68]. The demonstrated electric field directed movement of various cell types [23, 24, 29, 30, 47, 69-72] suggests the importance of electrotaxis and its potential physiological relevance and biomedical applications. The mechanisms of electrotaxis are not clearly defined, however, although some signaling pathways required for cell motility and chemotaxis such as PI3 Kinase, PTEN, and calcium signaling have been suggested to be involved in electrotaxis [3, 45]. Thus, further understanding the mechanisms of electrotaxis and identifying its new physiological roles as well as biomedical applications motivates a rapidly growing research area.

In conventional dished-based electrotaxis assays, electric fields are applied to a cell chamber in a petri dish containing medium through a pair of agar salt bridges, which prevent direct contact of electrodes with the cell culture and thus block the exposure to cells of possible electrode-derived toxic products [3, 23-27]. Then, the migration of cells in the cell chamber in response to the electric field can be monitored under a microscope. The dish-based assays have been widely employed to study electrotactic responses of different cell types [3]. Despite of the wide use of these sophisticated assays, the dish-based assays are limited in terms of the control of electric fields, experimental throughput and miniaturization.

In addition to the dish-based assays, a transwell-based electrotaxis assay was reported that allows multiple parallel electrotaxis experiments to be performed in a single well plate [29]. This assay is modified from the widely used transwell chemotaxis assay (that measures the number of cells migrated from the upper compartment to the bottom compartment through a thin membrane in response to the chemical gradient across the membrane. Here the assay is used to apply an electric field to cells by placing 2 electrodes in the upper and bottom compartments) and has been successfully used to identify electrotactic responses of different lymphocyte subsets and monocytes from human peripheral blood [29]. Comparing to the dish-based assay, the transwell assay has the advantage of the experiment throughput (in the well-plate format), ease of operation, and the capacity for post-assay analyses such as flow cytometry (because enough cells can be collected after the assay). However, the transwell assay is more suitable as an initial screening tool to identify possible electrotactic responses due to its limitations regarding electric fields uniformity of electric fields and as an endpoint assay that does not allow real-time visualization of cell movement vertically across the transwell.

In a study investigating electrotaxis in *Dictyostelium*, an electrotaxis device was developed consisting of a cell chamber formed by two coverslips separated by a specially designed silicon spacer [23]. This device has the similar setup with dish-based assay except it used a silicon spacer as the cell chamber. Electrotactic migration of *Dictyostelium* towards the cathode of an applied DC electric field over a field strength range of 0.25 V/cm to 10 V/cm was clearly demonstrated. These results further helped establish *Dictyostelium* as a model system for studying the general mechanisms of electrotaxis.

4.2 Microfluidic devices

In contrast to the above mentioned electrotaxis assays that apply electric fields to cells seeded in macro scale chambers, microfluidic devices have been recently developed for electrotaxis studies that apply electric fields to cells in micrometer-dimension channels of well-defined shapes [29-31, 33, 69, 73]. The well-defined microchannel geometry that avoids complicated boundary conditions for the electric field, therefore allowing better control of the uniformity and stability of the applied electric fields (Fig. 1-1B) [33], the Joule heating effect is reduced, and these devices have the potential for high-throughput experimentation. In this section, we highlight recent microfluidics-based electrotaxis studies with a focus on their biological relevance.

To examine electrotaxis of T lymphocytes, a plastic microfluidic electrotaxis device was developed (Table 4-1). The authors showed that memory T cells from human peripheral blood migrate toward the cathode of applied DC electric fields with the field strength comparable to it in wounded tissues [3, 29]. By intravital confocal imaging of GFP transgenic mouse skin tissues, the authors further demonstrated that T cell migration could be directed by applied electric fields *in vivo*. This is the first time that T cell electrotaxis is demonstrated both *in vitro* and *in vivo*, suggesting a new electrical guiding mechanism for lymphocyte migration and trafficking in tissues (in addition to the chemical based guiding mechanism) with possible relevance to physiological processes such as wound healing and immune responses.

Physiological electric fields can arise between cancerous tissues and neighboring normal tissues, and these fields can potentially promote and guide cancer cell migration [43]. Indeed, previous studies have demonstrated electrotaxis of different cancer cell types using conventional electrotaxis assays [24, 74]. A microfluidic device was developed to study the long-term electrotactic migration of lung cancer cells [69] (Table 4-1). More recently, a similar

microfluidic device was used to further demonstrate the biased growth of lung cancer cell filopodia toward the cathode of the external electric field as well as the polarized distribution of epidermal growth factor receptors (EGFRs that play important roles in mediating cancer growth and metastasis in tissues) toward the cathodal side (possibly caused by the electromigration of the receptors on the cell surface induced by the electric field) [73] as a potential mechanism. These results suggest that there is a correlation between lung cancer cell electrotaxis, metastatic potential, and the possible EGFR based cellular mechanisms. It will be very interesting and useful to further test the specificity of the EGFR mediated cancer cell electrotaxis.

The nematode *Caenorhabditis elegans* is a model organism for studying conserved biological processes with relevance to other biological species including human, owing to its useful features such as small size, transparency, short life cycle and the amenability for genetic manipulations [75]. In a recent study, a polydimethylsiloxane (PDMS) microfluidic device made by soft-lithography was developed to study electrotaxis in *C. elegans* [31] (Table 4-1). The results demonstrated the cathode-directing electrotaxis of *C. elegans* without affecting its survival and reproduction. In a more recent study, a simple agar gel-based device was used to demonstrate sorting *C. elegans* based on electrotactic mobility [76], and such studies can certainly be further pursued using microfluidic devices for better controlled electric field applications. Although exposure of *C. elegans* to electric fields in their living environments is not clear, the demonstrated electrotactic response of *C. elegans* provides a model system for further investigating the mechanisms of electrotaxis at the multi-cellular organism level - that can be completely different from the mechanisms operating at the cell level. On the other hand, it will be also interesting to compare the characteristics of electrotaxis between *C. elegans* and cells for possible similarities, and microfluidic devices can provide a platform for experimental analysis

and quantitative comparison.

More recently, a similar PDMS microfluidic device was used to study the orientation response of the fission yeast *Schizosaccharomyces pombe* in applied DC electric fields [30] (Table 4-1). The results show that the rod-shaped yeast reorients perpendicular to the applied electric field, producing cells with a bent morphology. Furthermore, a candidate genetic screen identified the involvement of an integral membrane protein ATPase, PMA1P, which regulates intracellular pH, the small GTPase CDC42P, and the formin FOR3P, which assembles actin cables, in regulating the electrotactic orientation of yeast, suggesting that one potential mechanism for the electrotactic response of yeast is through modulation of intracellular pH and polarity factors. Although *S. pombe* does not migrate but instead exhibits an orientation change in response to applied electric fields, a greater understanding of electric field-mediated yeast cell polarity could provide insight into mechanisms of electrotaxis. Notably, microfluidic devices have also been used recently to study chemotactic responses of yeast [77, 78], underlining the general applicability of microfluidic devices for studying yeast polarity in response to different guidance cues.

It is worth noting that the interactions between chemical gradients and electric fields, and their coexistence in tissues, suggest that complex guiding mechanisms are needed for accurate cell migration and movement. Studies investigating these mechanisms can be uniquely enabled by microfluidic devices allowing controlled chemical and electric fields.

Table 4-1: Microfluidic electrotaxis devices

1. Lin *et al.* [29] developed a plastic microfluidic electrotaxis device containing a 500 μm (W) × 15 mm (L) × 100 μm (H) laser-cut straight microchannel to study electrotaxis of human blood memory T cells. Two pipette tips were cut and glued to the channel wells to serve as medium reservoirs, in which electrodes were inserted to apply the electric field.
2. Huang *et al.* [69] developed a microfluidic device in a polymethylmethacrylate (PMMA) sheet to study lung cancer cell electrotaxis. The device consists of multiple interconnected layers of microchannels with wells on the top of the device assembly for medium inlet/outlet and agar bridge insertion to apply the electric field. Three different sizes of segments were sequentially aligned in the microchannel such that the device can uniquely generate electric fields with three different strengths all in a single microfluidic channel, suggesting the potential for high-throughput experiments.
3. Rezai *et al.* [31] reported a microfluidic device for studying electrotaxis in *C. elegans*. The device was fabricated in PDMS and consists of a straight channel with wells at both ends for introducing *C. elegans* and medium and for applying electric fields.
4. Minc *et al.* [30] used a similar PDMS microfluidic device to study the orientation response of the fission yeast *Schizosaccharomyces pombe* in applied DC electric fields. This device uses agarose-containing medium blocks at the two ends of the channel to protect cells in the channel from potentially toxic by-products emanating from the electrodes.

For all types of microfluidic electrotaxis devices, cells or organisms are loaded into the microfluidic channel and their movement or orientation in response to the applied electric field is visualized and recorded by time-lapse microscopy.

Chapter 5

General methodologies

5.1 Microfluidic device preparation

5.1.1 Device design

The microfluidic electrotaxis and chemotaxis devices are designed using Freehand 9.0 (Macromedia). The width of the main cell channel depends on the size and the migration speed of the cells for effective cell migration monitoring. For lymphocytes with the typical size of approximately 10 μm in diameter and migration speed of approximately 10 μm/min, a few hundred micrometers is often used for the width of the main channel. In our study, the width of main channel is 350 μm for all devices. The completed designs are printed to a transparency mask with a high-resolution printer (2400 dpi).

5.1.2 Photolithography

Photolithography (also called optical lithography) is a process that uses UV light to transfer a geometric pattern from a mask to photoresist on the substrate. The photoresist can be divided into two categories: 1) positive photoresists, for which the exposed areas are dissolved in the developer, leading to photoresist patterns similar to the image of the mask; 2) negative photoresists, for which exposed areas become insoluble in the developer and give the photoresist patterns that are the complementary image of the designed mask. In our study, we used negative photoresist SU-8 2025 to achieve the desired microchannel thickness (~100 μm).

5.1.3 Soft-lithography

Soft lithography is a collection of techniques for printing or replicating structures using elastomeric stamps, most commonly polydimethylsiloxane (PDMS) [79], and is generally used

to construct features measures on the micrometer to nanometer scale and generally compatible with biological applications. Compared with the inorganic materials such as silicon and glass that are used in microelectronics and optics, PDMS offers a number of unique and attractive features for biologically directed microfluidics, such as optical transparency, cost efficiency and biological compatibility.

5.1.4 Fabrication procedures of microfluidic devices

In our study, the designs are negatively patterned on a silicon wafer by contact photolithography with SU-8 2025 photoresist (MicroChem, MA) at The Nano Systems Fabrication Laboratory (NSFL) at The University of Manitoba. The detailed fabrication procedures are illustrated in Fig. 5-1. The key steps for fabrication of our substrate include: **1) Substrate preparation:** before the photolithography process, the substrates (3 inch silicon wafers in our study, Silicon Inc., Boise, Idaho, USA) are cleaned with piranha (using H_2SO_4 & H_2O_2) followed by a de-ionized water rinse; **2) Spin coating:** dispense 3 mL of photoresist at the center of the silicon wafer; spin at 500 rpm for 5 seconds with acceleration of 100 rpm/s; spin at 2000 rpm for 30 seconds with acceleration of 300 rpm/s; **3) Soft bake**: place the resist coated wafer on a level hotplate for 5 min at 65 °C and 20 min at 95 °C to dry off excessive photoresist solvent; **4) UV exposure:** put the wafer under the UV machine and with the transparency mask on top of the wafer; turn on the UV and leave it on for 20 seconds; **5) Post-exposure bake (PEB):** place the exposed wafer on the hotplate (same as the one used in soft bake) for 5 min at 65 °C and 10 min at 95 °C to facilitate polymerization of the photoresist; **6) Development:** the unexposed SU-8 will be washed off in the SU-8 developer for about 10 min; **7) Rinse and dry:** after developing, rinse the wafer using de-ionized water and use a N_2 gas gun to remove residual photoresist on the wafer; **8) Hard bake:** place the cleaned wafer on hotplate for a couple of minutes at 150 °C to

ensure that the photoresist properties do not change (SU-8 2025 is a thermal resin and as such its properties can continue to change when exposed to higher temperature than previously encountered) and to enhance resist adhesion to the wafer.

After the optical lithographic steps, the silicon master is stamped to PDMS (Sylgard 184, Dow Coring, MI) with the standard soft-lithography technique. After 3 h of baking at 70 °C in an oven, the PDMS replica is cut and detached from the silicon wafer, the designed geometry is transferred from the silicon master to the PDMS. Inlets and outlets for the fluids and cells are punched out with sharpened needles. Then place the PDMS stamp (with the patterned surface facing up) and a clean glass substrate in an air plasma cleaner (PDC-32G, Harrick, NY) for 1 min and immediately bond the PDMS to the glass substrate to form an irreversible seal. This step also helps clean the PDMS surface and the glass slide and modifies PDMS surface to hydrophilic. The completed microfluidic device is wetted by filling with DI water to preserve hydrophilicity of the PDMS channels. The fabrication process of microfluidic devices is illustrated in Fig. 5-1.

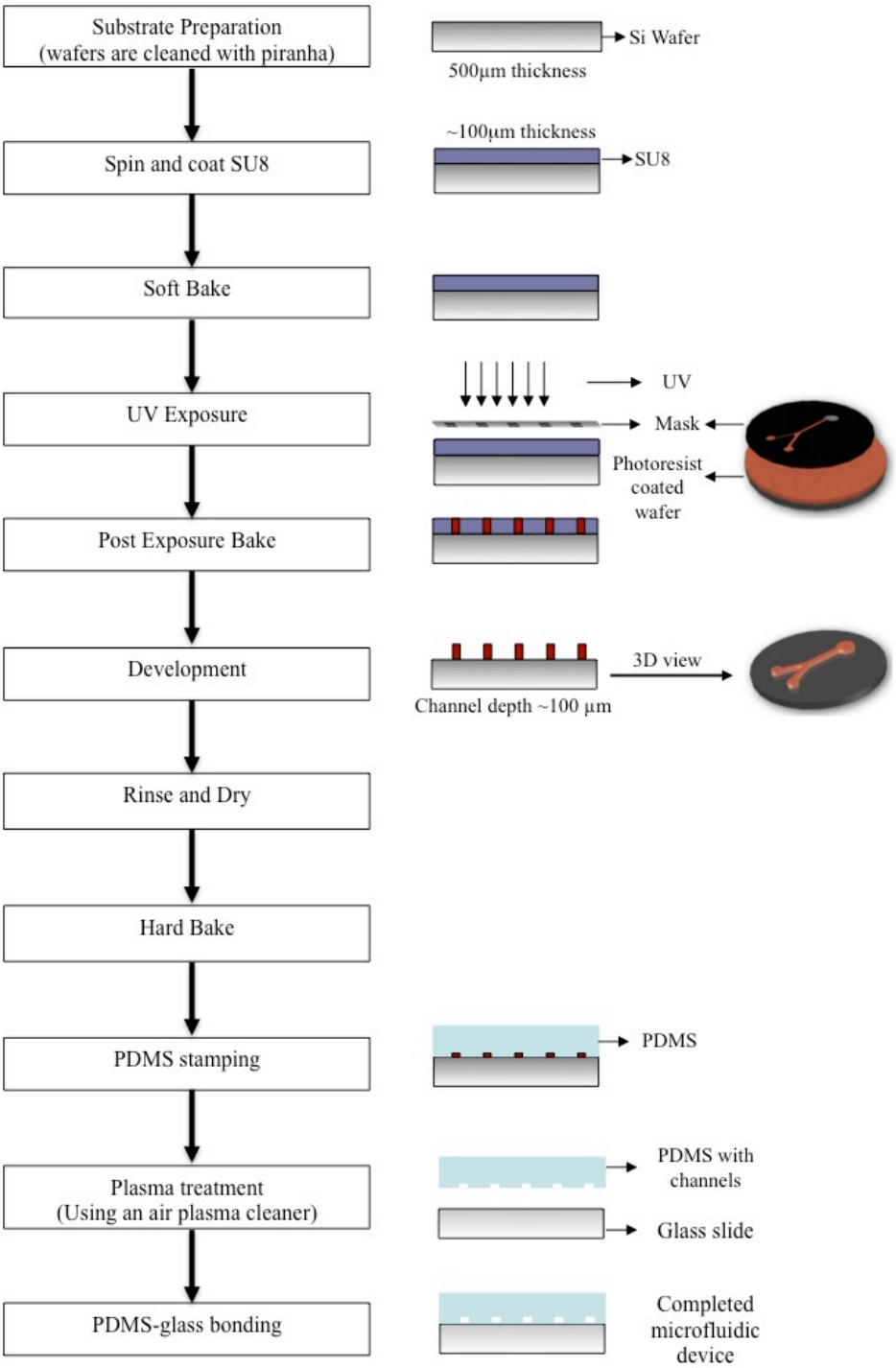

Fig 5-1. Illustration of photolithography and soft-lithography.

5.2 Cell preparation

Preparation of activated T cells is illustrated in Fig. 5-2. Briefly, human peripheral blood mononuclear cells (PBMC) were isolated from whole blood from healthy blood donors in collaboration with The Victoria General Hospital at Winnipeg, using the standard gradient centrifugation method. Isolated PBMC were washed with Phosphate buffered saline (PBS) several times. T cells in total PBMC were selectively activated by incubation in culture medium (RPMI-1640 with 10 % FBS) with anti-CD3/CD28 antibodies in a 37 °C incubator with 8 % CO_2 injection for 2 days. After the activation, cells in the solution were transferred to a new flask and cultured in the presence of IL-2 for at least 3 days before cell migration experiments. The purity of T cells was measured by flow cytometric analysis of CD3 expression (Fig. 5-2B).

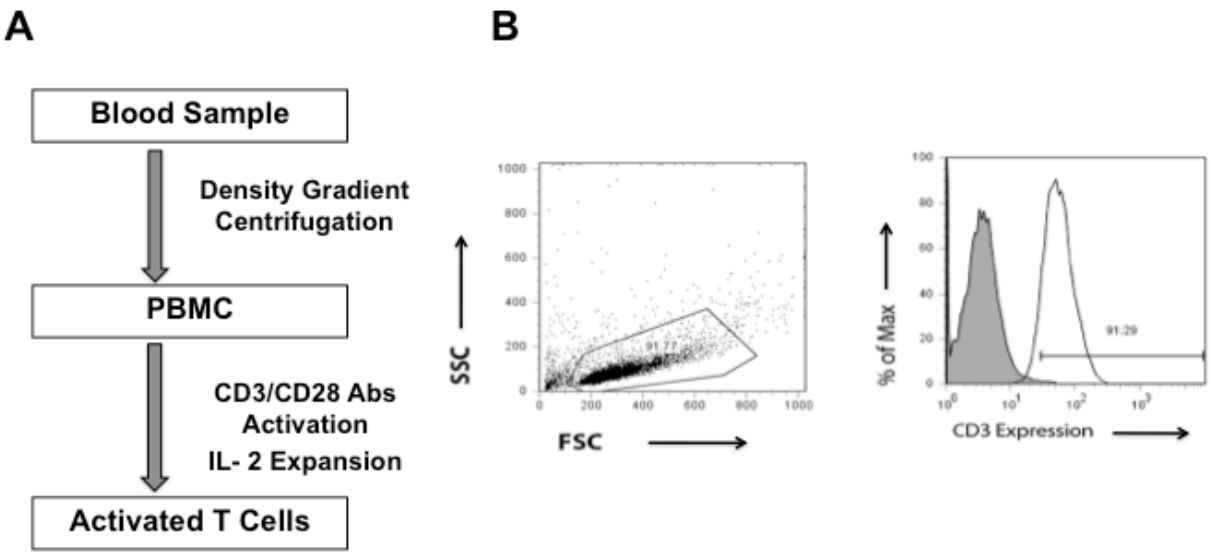

Fig 5-2. Illustration of cell preparation. *(A) Flow chart of activated T cell preparation. (B) Flow cytometry confirms that the majority of the cells used are CD3+ T cells. Cells are gated for the lymphocyte population (left panel) before CD3 expression analysis (right panel). The shadowed curve in the right panel is the control sample [33]. Reproduced with permission from Royal Society of Chemistry (RSC).*

5.3 Experimental setup

To provide a substrate for cell adhesion and migration, the fluidic channel is coated with fibronectin (Human Fibronectin, BD Biosciences, MA) for 1 hour at room temperature and then blocked with Bovine serum albumin (BSA) for another hour before the experiment. Briefly, for each experiment, a few thousand cells are loaded into the microfluidic device from the wells and allowed to settle in the fibronectin-coated channel for ~5 min. The device is maintained at 37 °C by attaching a transparent heater to the back of the coverslide (Thermal-Clear Transparent Heater, Model No. H15227, Minco, MN). The heater is powered by a DC power supply (Model No. 6204A, Harrison, Canada) and is controlled by a sensorless temperature controller (Model No. CT198, Minco, MN). The temperature is calibrated to 37 °C using a digital thermometer (VWR, Canada). However, the experimental setup in different studies may vary slightly. Cell movements in the microfluidic devices are recorded by time-lapse microscopy over the defined experiment period.

5.4 Data analysis

Movement of individual cells is tracked using NIH ImageJ (v.1.34s). The background noise of the image is removed using the "despeckle" function. Then the images are calibrated to distance. Only the cells that migrated within the microscope field were selected and tracked using the "Manual Tracking" plug-in in NIH ImageJ. The tracking data were exported to Excel and Oriana or Origin for analysis. At least 30 cell tracks from multiple independent experiments were analyzed.

Following previously established analysis methods, the movement of cells was quantitatively evaluated by (1) **the percentage of cells** that migrated toward the cathode of the electric field for

electrotaxis experiments, or toward CCL19 gradient in chemotaxis experiments; (2) **Orientation Index (O.I.)**, which is the ratio of the displacement of cells toward the cathode of the electric field in electrotaxis experiments (Δx or Δy, depends on the DC electric field direction in different microfluidic devices) or toward the CCL19 gradient in chemotaxis experiments (Δy), to the total migration distance (d) using the equation O.I. = $\Delta y/d$ or $\Delta x/d$, presented as the average value ± standard error of the mean (SEM); (3) **the motility index (M.I.)**, defined as normalized cell displacement and presented as the average value ± SEM of all cells; (4) **the average speed (*V*)** calculated as $d/\Delta t$ and presented as the average value ± SEM of all cells; and (5) statistical analysis of migration angles performed using Oriana for Windows (Kovach Computing Services) or Origin to examine the directionality of the cell movement. Specifically, migration angles (calculated from x-y coordinates at the beginning and the end of the cell tracks) were summarized in a direction plot, which is a rose diagram showing the distribution of angles grouped in 20° intervals, with the radius of each wedge indicating cell number.

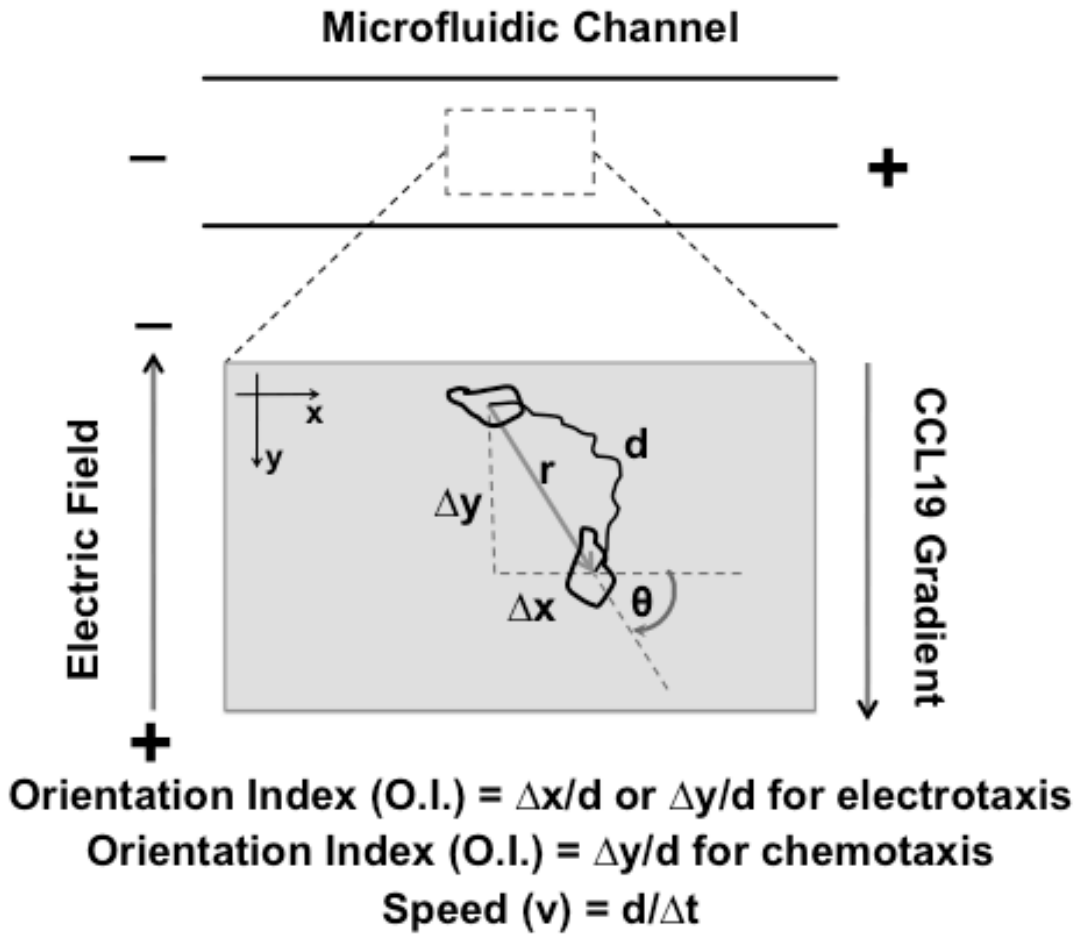

Fig 5-3. Illustration of microfluidic cell migration data analysis.

5.5 COMSOL multiphysics modeling

In order to characterize the chemical gradients and electric field in the microfluidic devices, multiphysics modeling and computer simulations were performed using COMSOL Multiphysics (v3.4 for the study in Chapter 6, and v4.2 for the study in Chapter 7). The detailed simulation methods will be discussed later in these chapters.

Chapter 6

T cell migration in specific microfluidic chemotaxis and electrotaxis devices

6.1 Introduction

The importance of electrotaxis and the assays for studying electrotaxis were discussed in previous chapters of this thesis. Comparing to the commonly used dish-based electrotaxis assay [25], microfluidic devices have the advantages of miniaturization and the control of electric field application to cells [28]. Recently, a simple plastic microfluidic device was employed for studying electrotaxis of memory T cells from human peripheral blood [29]. However, further utilization of such a device is hindered by the poorly controlled channel shape and potential toxicity to cells resulting from epoxy gluing of medium wells to the channel. To overcome these limitations, in the present study, we employed a PDMS-based and a glass-based microfluidic device and successfully demonstrated electrotaxis of activated human blood T cells [33]. The PDMS and glass devices are complementary in their ease of prototyping and use (PDMS device), and the control of electric fields with integrated on-chip electrodes (glass device). Furthermore, the results from the PDMS device allow direct comparison of electrotaxis of activate T cells with chemotaxis of the same cell type. Given the importance of activated T cells in the adaptive immune responses, our results suggest that not only resting lymphocytes can be stimulated and directed by electric fields; the migration of activated lymphocytes can also be electrically manipulated with the potential to more closely mediate immune responses.

6.2 Methodology

6.2.1. Cell preparation

Preparation of activated T cells is described previously [32](Chapter 5.2).

6.2.2. Microfluidic device preparation

6.2.2.1 PDMS electrotaxis and chemotaxis devices

The general fabrication method of PDMS microfluidic devices has been described previously (Chapter 5.1).

For the electrotaxis device (Fig. 6-1), 2 wells (4 mm diameter holes) at the 2 ends of a 350 μm (W) x 1cm (L) channel were punched out using sharpened needles. The surface of the PDMS replica and a clean glass coverslide were treated with air plasma for 1 min using a plasma cleaner (PDC-32G, Harrick, NY) and brought together to form an irreversible seal. This assembly produced the required systems of microfluidic channel. External platinum electrodes (SPPL-010, Omega Engineering, Inc) that were attached to conducting wires were inserted into two medium reservoirs and the wires were connected to a DC power supply to apply electric field to the microchannel. A new microfluidic device was used for each experiment.

The "Y" shape chemotaxis device has been described in details previously [32] (Fig. 6-2). The fabrication procedures and the channel dimensions are identical to the electrotaxis device. Instead of 2 wells at the 2 ends of the channel as in the electrotaxis device, two 1 mm diameter holes for the 2 fluidic inlets and one 4 mm diameter hole for the fluidic outlet were punched out respectively in the PDMS chemotaxis device. Polyethylene tubing (PE-20, Becton Dickinson, MD) was inserted into the inlet holes to connect the microfluidic device to syringe pumps (Model V6, Kloehn, Inc., NV) with two 250 μL Kloehn syringes containing medium or chemokine solution for fluidic infusion.

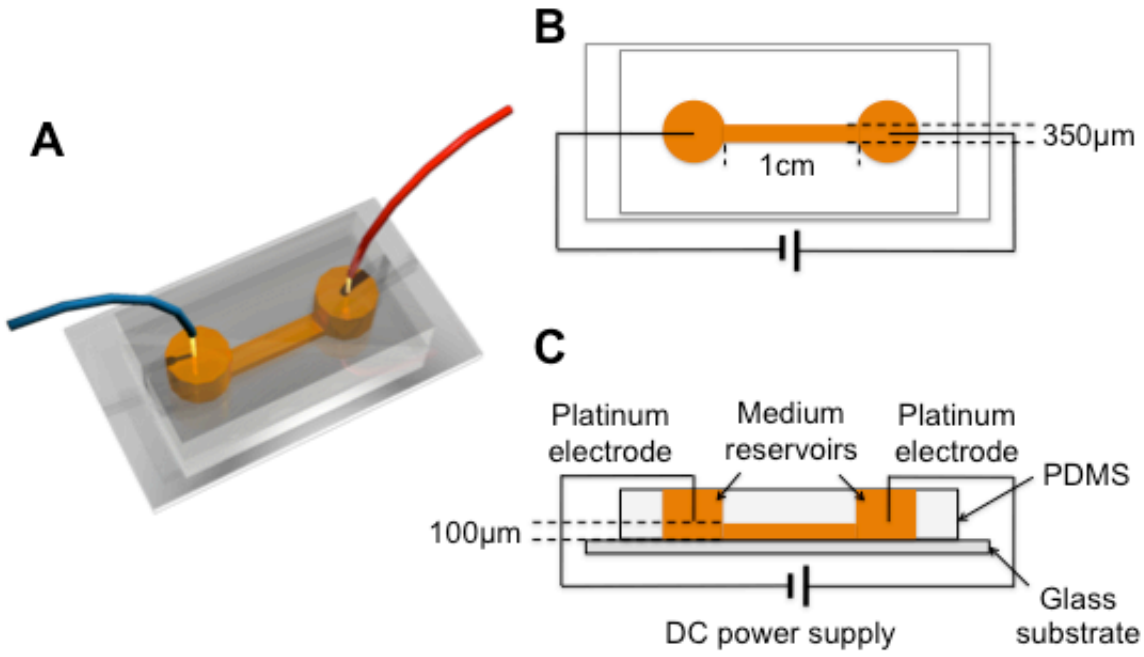

Fig 6-1. Illustration of the PDMS microfluidic electrotaxis device. *(A) 3D schematic drawing of the PDMS microfluidic electrotaxis device. (B) Top view of the PDMS microfluidic electrotaxis device. (C) Side view of the PDMS microfluidic electrotaxis device. Reproduced with permission from Royal Society of Chemistry (RSC).*

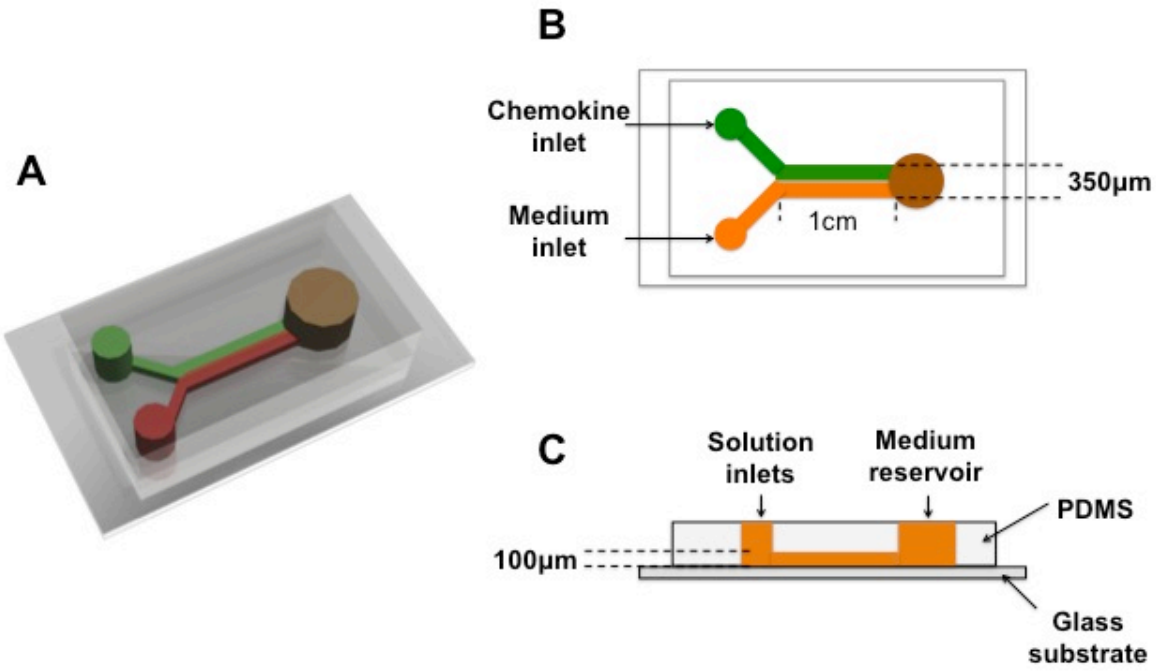

Fig 6-2. Illustration of the "Y" shape microfluidic chemotaxis device. *(A) 3D schematic drawing of the chemotaxis device. (B) Top view of the chemotaxis device. (C) Side view of the chemotaxis device.*

6.2.2.2. Glass electrotaxis device

The channel mask and the electrode mask used to fabricate the glass device were designed using Cadence's Custom IC Design Tools Virtuoso® Front to Back Design Environment (IC 5.1.41). The design was collected by the Canadian Microelectronics Corporation (CMC), and then submitted to Micronit for fabrication using their Sensonit Glass-Based Microfluidic Technology with Metallization process. The fabrication process begins by first etching the 40 μm deep microfluidic channels into the bottom side of a glass wafer, using the channel mask for boundary definition. A wet isotropic etch was used to create the 500 μm wide channel connecting the fluid ports. The glass wafer's top was then powder-blasted to create the fluid ports and the electrode coupling trench, using the powder-blast mask for boundary definition. The fluid ports have 2 mm top and 1.2 mm bottom diameters. 200 nm deep trenches were then etched into the topside of a second glass wafer, using the electrode mask for boundary definition. An array of 200 μm wide platinum electrodes was then deposited into these trenches. The two glass wafers were then fused together using a direct heat bond. Microfluidic device fabrication was then completed by cutting the fused glass wafers to yield each individual die. Then the electrodes were connected to external wires using conducting glue for electric field application to the channel. A piece of PDMS with two wells aligned with the fluid ports of the glass device was plasma bonded to the topside of the glass device for easy fluid addition. Fig. 6-3 shows the schematic drawing of the glass electrotaxis device. For easy illustration, the channel shape and the electrode array are simplified in the drawing without affecting the key features of the design. In addition, the top PDMS layer is not shown. The curved channel is due to the size limit of the Micronit fabrication process and the requirement of channel length for application of low electric fields.

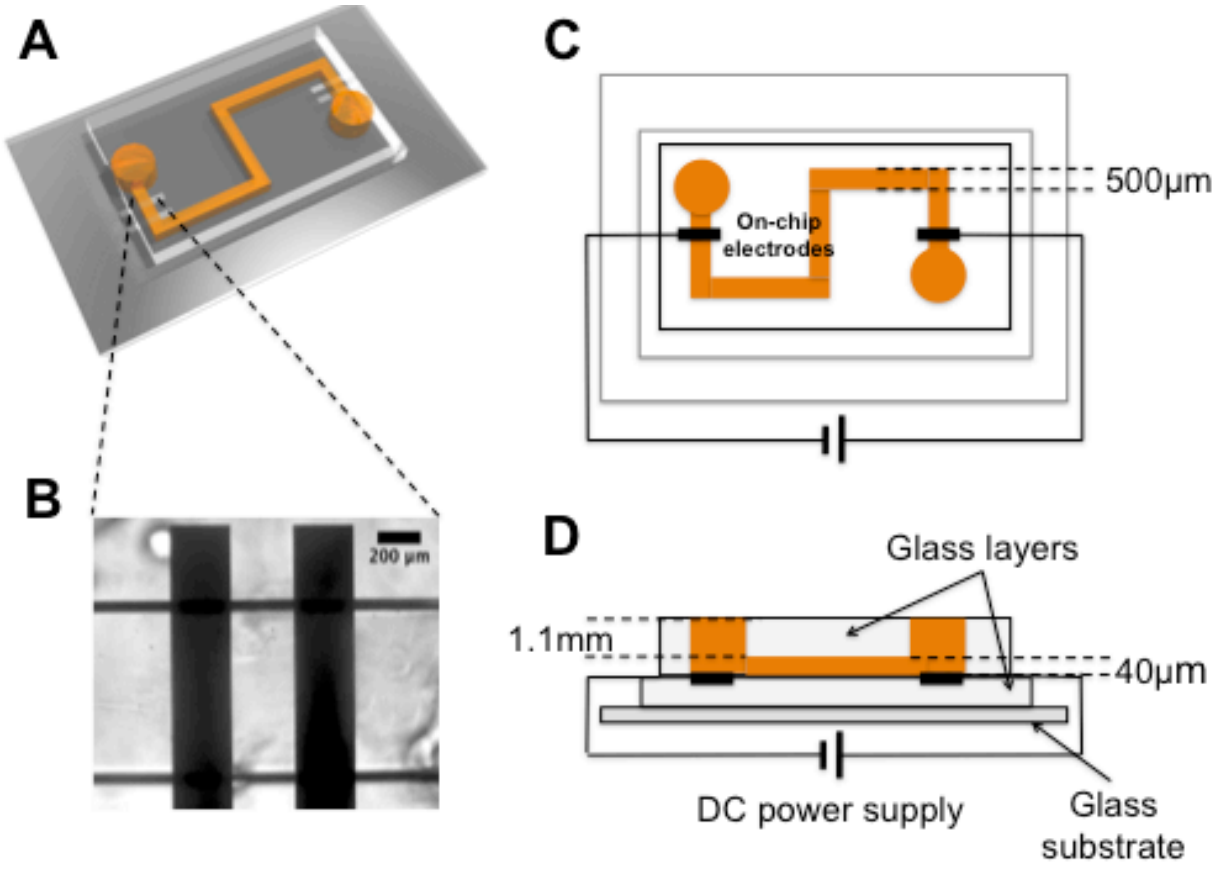

Fig 6-3. Illustration of the glass microfluidic electrotaxis device. *(A) 3D schematic drawing of the glass microfluidic electrotaxis device. (B) Image of on-chip electrodes (black) across the microchannel. (C) Top view of the glass microfluidic electrotaxis device. (D) Side view of the glass microfluidic electrotaxis device. Reproduced with permission from Royal Society of Chemistry (RSC).*

6.2.3 Cell migration experiment

The fluidic channel was coated with fibronectin (Human Fibronectin, BD Biosciences, MA) for 1 hour at room temperature and blocked with BSA for another hour before the experiment. The experimental setup of the cell migration experiment is illustrated in Fig. 6-4. Briefly, for each experiment, a few thousand cells were loaded into the microfluidic device from the wells and allowed to settle in the fibronectin-coated channel for ~5 min. The device was maintained at 37 °C by attaching a transparent heater to the back of the coverslide (Thermal-Clear Transparent Heater, Model No. H15227, Minco, MN). The heater was powered by a DC power supply (Model No. 6204A, Harrison, Canada) and was controlled by a sensorless temperature controller (Model No. CT198, Minco, MN). The temperature was calibrated to 37 °C using a digital thermometer (VWR, Canada). After the cells were settled in the channel, ~150 μL of medium (RPMI 1640 with 0.4 % BSA) was added to each well for electrotaxis experiments. For the PDMS electrotaxis device, two platinum electrodes (0.25 mm in diameter; Omega) connecting to a DC power supply (Model No. 2555A, Central Scientific, NY) were placed in the medium wells to complete the circuit. For the glass electrotaxis device, electric field was directly applied to the channel through the on-chip electrodes. If needed, more medium was added to the wells during the experiment. For the PDMS chemotaxis device, medium and chemokine solutions were infused into the device by syringe pumps through tubing and the inlets of the device. The device was placed on a microscope stage (Model No. BX60, Olympus). For electrotaxis experiments, the system was allowed to equilibrate for ~ 5 min (wait until no flowing cells were seen in the channel). Then, the DC electric field was applied, and cell migration was recorded by time-lapse microscopy at 6 frames/min for 20 min using a CCD camera (Model No. 370 KL 1044, Optikon, Canada). The image acquisition was controlled by NIH ImageJ (v.1.34s). For chemotaxis

experiments, the medium and chemokine solutions were infused into the device at the total flow rate of 0.2 μL/min. The chemokine gradient was confirmed by measuring the fluorescence intensity profile of FITC-Dextran 10 kD that has similar molecular weight of the chemokine molecule and was added to the chemokine solution, inside the microfluidic channel. The cells were imaged at ~3 mm downstream of the "Y" junction where the gradient yields a smooth profile.

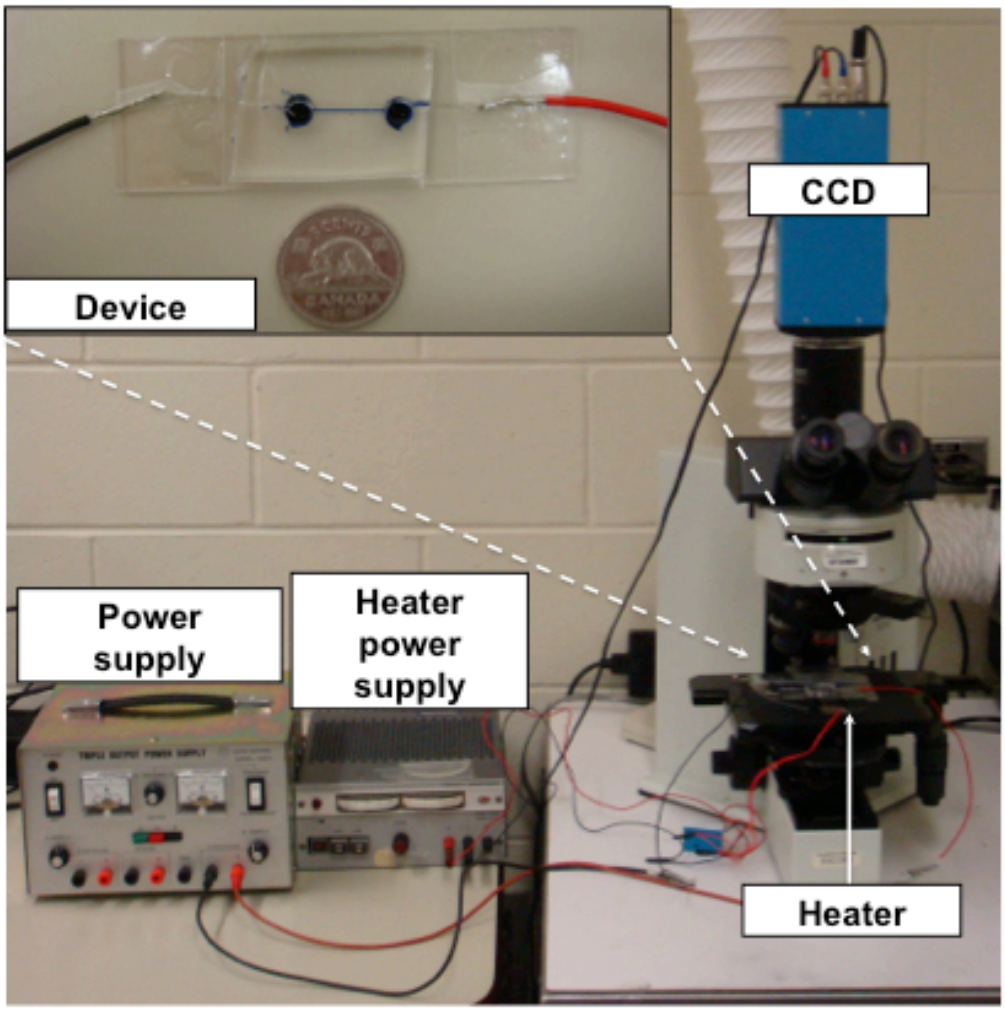

Fig 6-4. Cell migration experimental setup. *Microfluidic device was placed on a microscope stage; a transparent heater powered by a power supply was attached to the back of the device to provide temperature control through an on/off temperature controller; electrodes connected to a power supply were connected to the device; cell migration images in the device was recorded through a CCD camera. A picture of a real device with electrode connection is shown. Blue dye was injected to the device to visualize the channel. Reproduced with permission from Royal Society of Chemistry (RSC).*

6.2.4 Data analysis

Movement of individual cells was tracked using NIH ImageJ (v.1.34s). The detailed methods were introduced previously (Chapter 5.4). Specifically, in this study, migration angles (calculated from *x*-*y* coordinates at the beginning and the end of the cell tracks) were summarized in a direction plot, which is a rose diagram showing the distribution of angles grouped in 20° intervals, with the radius of each wedge indicating cell number. The Rayleigh test for circular uniformity was applied, with a significance level of 0.05. When there was significant directionality, the mean angle and the 95 % confidence interval were calculated. A modified Rayleigh test (V test) was also applied, to test whether deviations from the direction of electric field (180 degrees) or the CCL19 gradient (90 degrees) were significant. For cell tracks figures (Fig. 6-7D & 6-9D), we used CellTrack (Ohio State University) for detecting cell boundaries, and exported the data to Origin for plotting.

6.3 Results

6.3.1. Electrotaxis and chemotaxis of activated T cells in PDMS microfluidic device

As described in the Materials and Methods section, the PDMS electrotaxis device (Fig. 6-1) consists of a single straight channel with two wells at the ends of the channel as medium reservoirs. The electrodes were inserted to the medium reservoirs to apply the electric field to the channel. This device is in principle similar to a previously reported microfluidic device for studying electrotaxis of *Caenorhabditis elegans*. Compared with the previously reported plastic microfluidic electrotaxis device, the current device inherited the features of PDMS devices in well-defined channel shape, optical transparency, cell compatibility, gas permeability and low fabrication costs.

Using this PDMS device, we generated a DC electric field of ~7 V/cm in the microfluidic channel. The measured current (34 μA) is consistent with the simulated current density (Fig. 6-5), and we tested electrotaxis of activated human peripheral blood T cells over the 20 min experiment period. Furthermore, computer simulations show that the electric field and current density are uniform in the microfluidic channel where cell migration is imaged (Fig. 6-5). This electric field strength induced the optimal electrotactic orientation of cells toward the cathode of the field for the range of electric field tested (Fig. 6-7) and thus was used for further quantitative analysis and comparison with chemotaxis. Our results show clear electrotaxis of activated human peripheral blood T cells toward the cathode of the electric field over 20 min experiment period (Fig. 6-7). In the absence of the electric field, cells exhibited random migration.

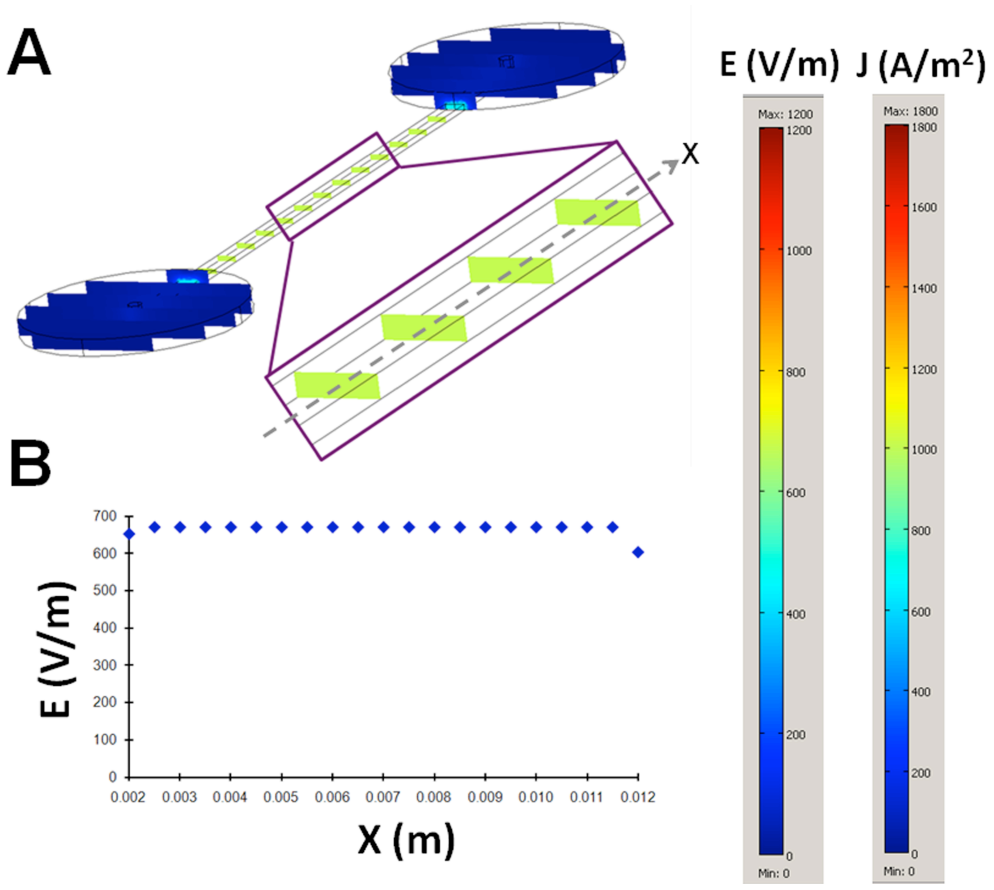

Fig 6-5. Simulation of dcEF in the PDMS microfluidic electrotaxis device. *(A) Simulated electric field and current density inside the microfluidic channel. (B) Plot of simulated electric field along the length of the channel. The electric field is uniform except the region close to the medium reservoirs. Reproduced with permission from Royal Society of Chemistry (RSC).*

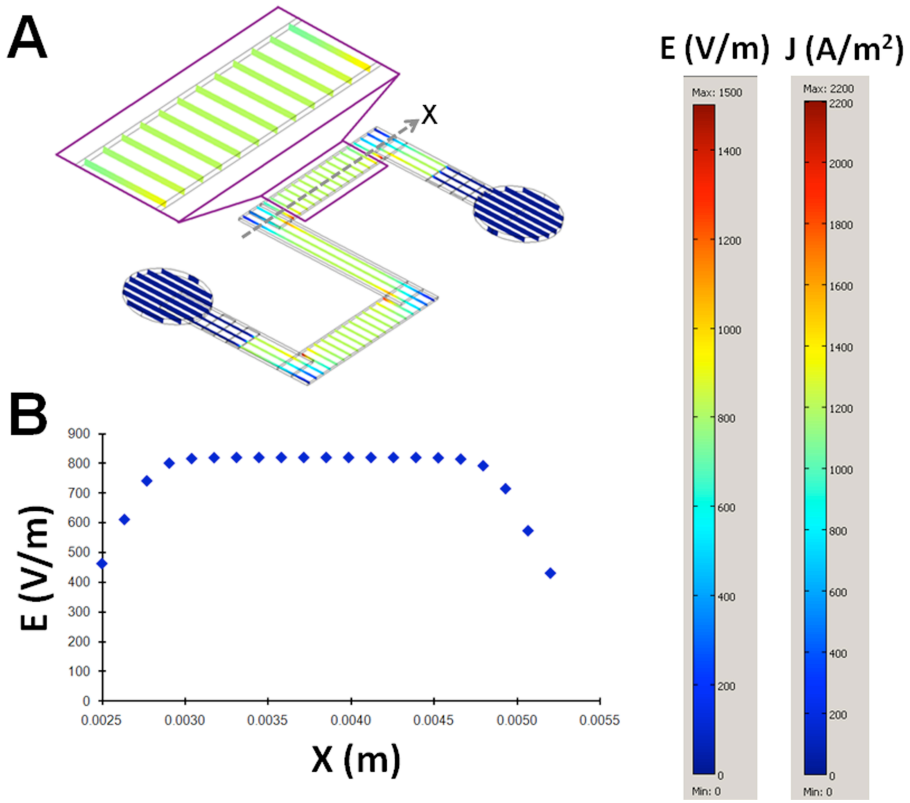

Fig 6-6. Simulation of dcEF in the glass microfluidic electrotaxis device. *(A) Simulated electric field and current density inside the microfluidic channel. (B) Plot of simulated electric field along the length of the channel between the turnings. The electric field is uniform in the straight region of the channel. Reproduced with permission from Royal Society of Chemistry (RSC).*

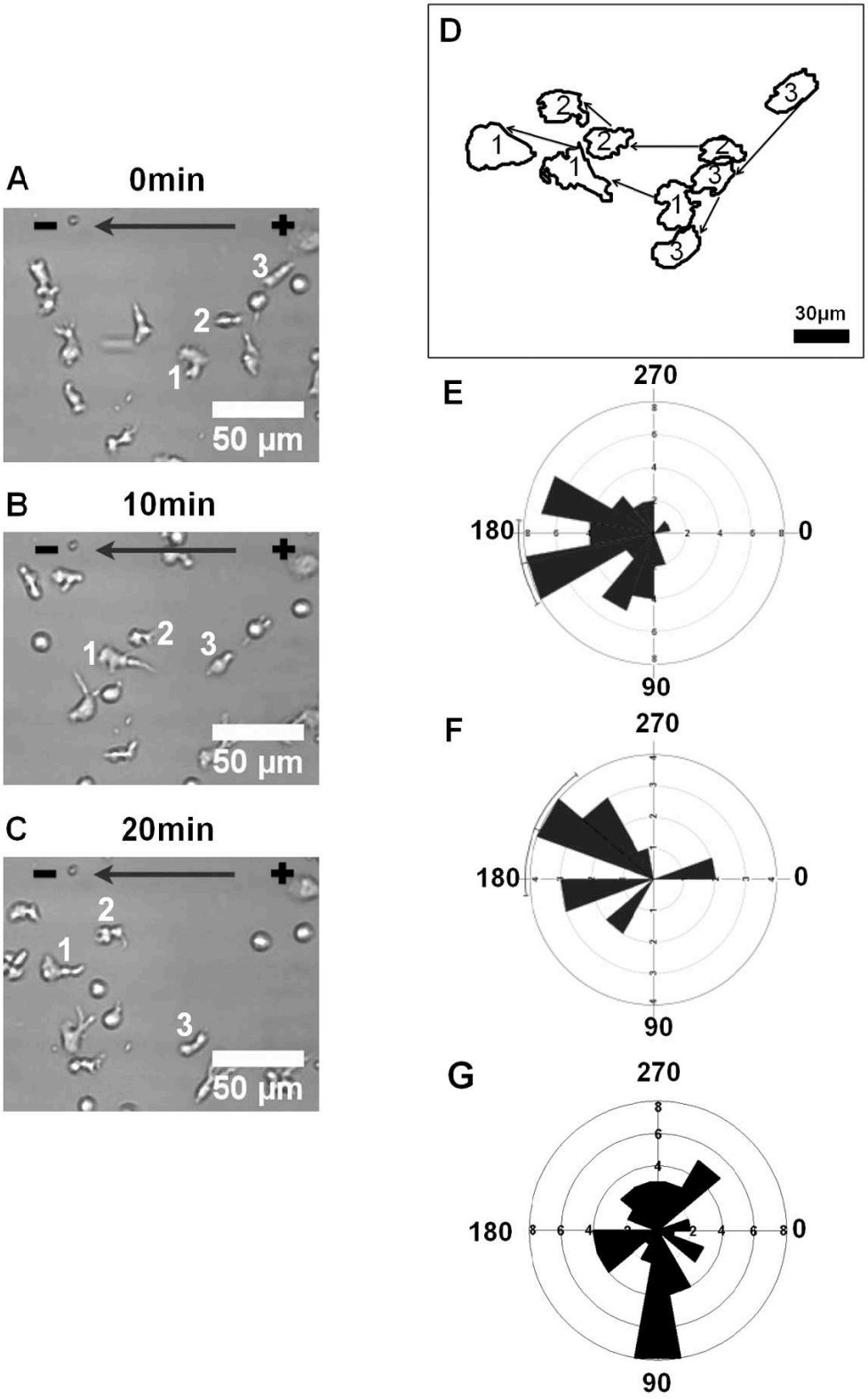
A
0min
50 µm
B
10min
50 µm
C
20min
50 µm
D
30µm
E
270
180
0
90
F
270
180
0
90
G
270
180
0
90

Fig 6-7. Electrotaxis of activated T cell in microfluidic devices. *(A-C) Time-lapse micrographs of cells in an applied electric field inside the PDMS microfluidic device at 0 min, 10 min and 20 min of the experiment. Three representative electrotaxing cells were labeled. (D) Migration tracks of the three representative cells. The rose diagram (E for PDMS device with the electric field; F for glass device with the electric field; G for medium control without electric field application.) shows the distribution of migration angles of all cells analyzed from representative experiments (the migration angles were calculated from x-y coordinated at the beginning and the end of the cell tracks, and were grouped in 20° intervals, with the radius of each wedge indicating cell number). Multiple independent repeating experiments were performed for each condition. Reproduced with permission from Royal Society of Chemistry (RSC).*

Using a previously described “Y” shape PDMS microfluidic device, we measured the migration of activated T cells in a 100 nM chemokine CCL19 gradient over the same 20 min experiment period as in the electrotaxis experiments and we showed robust CCL19 gradient induced chemotaxis of activated T cells (Fig. 6-9, Table 6-1). This 100 nM CCL19 gradient induced the optimal chemotactic orientation compared to other CCL19 gradients tested at a lower or higher dose (Fig. 6-8) and thus this 100 nM CCL19 gradient was used for further comparison with electrotaxis.

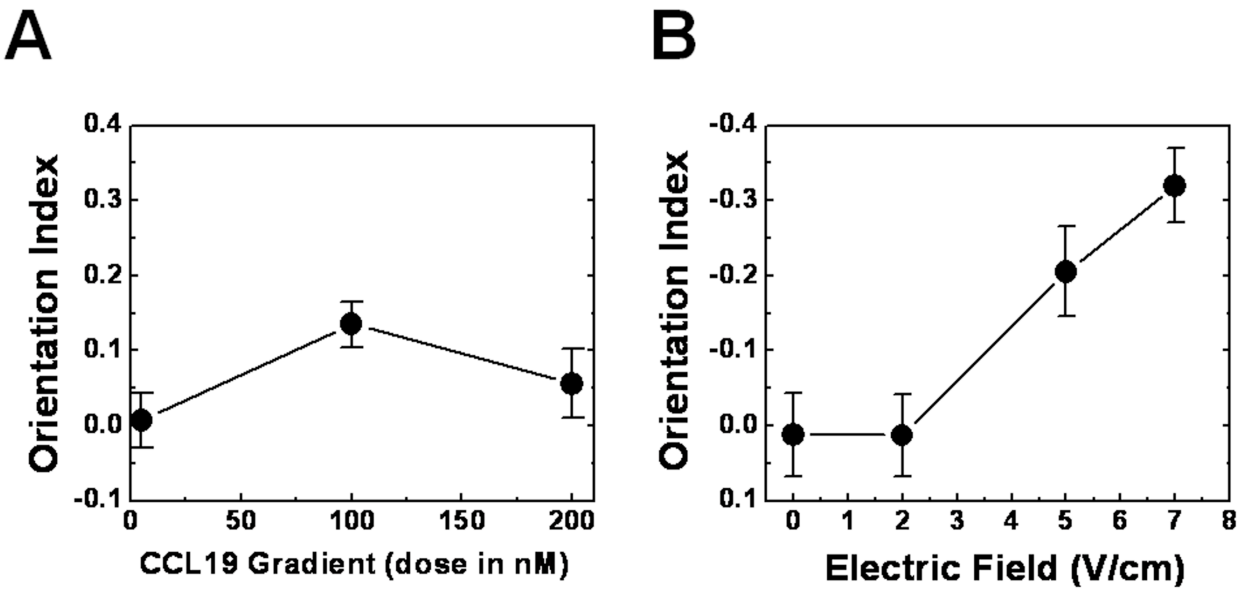

Fig 6-8. T cell migration in chemical gradients and dcEF in the PDMS microfluidic devices. *(A) Orientation Index in different CCL19 gradients. The optimal chemotactic response occurs in the 100nM CCL19 gradient. (B) Orientation Index in different electric fields. The optimal electrotactic response occurs in the 7V/cm electric field. Thus, the cell migration data in the 100nM CCL19 gradient and the 7V/cm electric field were used for further analysis and comparison. Reproduced with permission from Royal Society of Chemistry (RSC).*

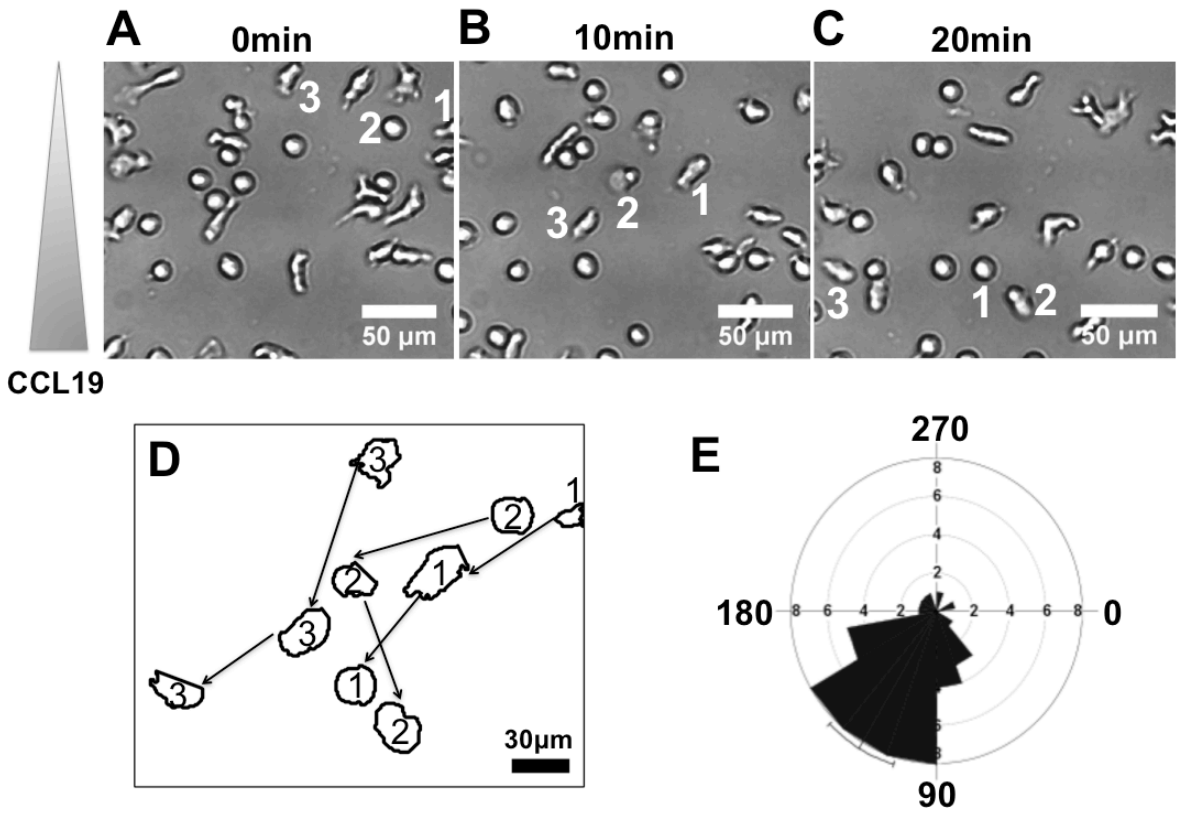

Fig 6-9. T cell chemotaxis in the PDMS microfluidic device. *(A-C) Time-lapse micrographs of cells in a CCL19 gradient inside the microfluidic channel at 0 min, 10 min and 20 min of the experiment. Three representative chemotaxing cells were labeled. (D) Migration tracks of the three representative cells. (E) The rose diagram shows the distribution of migration angles of all cells analyzed (n=45) from 1 representative experiment (the migration angles were calculated from x-y coordinates at the beginning and the end of the cell tracks, and were grouped in 20° intervals, with the radius of each wedge indicating cell number). The flow is toward the left. Reproduced with permission from Royal Society of Chemistry (RSC).*

The similarities of the PDMS electrotaxis and chemotaxis devices allow quantitative comparison between electrotaxis and chemotaxis of activated T cell. As summarized in Table 6-1, activated T cells exhibited comparable or even higher orientation and motility responses in the 7 V/cm electric field compared to in 100 nM CCL19 gradient. To our best knowledge, these analyses are the first direct comparison of electrotaxis and chemotaxis of the same cell type in similar microfluidic device (both the electrotaxis device and the chemotaxis device were made in the PDMS using identical fabrication methods and that the dimension of the channel for observing cell migration is the same).

The main limitation of the current PDMS electrotaxis device is the lack of control of positioning external electrodes in the medium reservoirs that may complicate the experimental conditions. The electrodes and wires often move or fall off the device during the experiments and we had to exclude these experiments for analysis. To overcome this limitation, we next repeated the electrotaxis experiments using the glass microfluidic device with integrated on-chip electrodes.

6.3.2. Electrotaxis of activated T cells in glass microfluidic device with integrated electrodes

As described in the Materials and Methods section with details, the glass microfluidic device consists of integrated on-chip electrodes across the microfluidic channel for application of electric fields (Fig. 6-3). Computer simulation shows that the electric field and current density are uniform in the straight region of the microfluidic channel where cell migration is imaged (Fig. 6-6). Using this device, we repeated the electrotaxis experiment with activated human T cells. Our results show similar electrotactic migration of cells toward the cathode of the applied electric field (Fig. 6-7F; Table 6-1).

	% of Chemotaxing or Electrotaxing Cells	Orientation Index	Speed (μm/s)	Motility Index	n
Electrotaxis in Glass Device	86.7	-0.23 ± 0.05	0.17 ± 0.01	0.34 ± 0.03	26
Electrotaxis in PDMS Device	90.5	-0.32 ± 0.05	0.16 ± 0.01	0.53 ± 0.04	47
Chemotaxis in PDMS Device	75.5	0.14 ± 0.03	0.15 ± 0.01	0.39 ± 0.02	94
Medium Control	47.9	-0.01 ± 0.05	0.11 ± 0.01	0.38 ± 0.02	48

Table 6-1. Quantitative comparison of chemotaxis and electrotaxis of activated T cells in microfluidic devices. *The parameters were calculated using cell tracks from multiple independent experiments. Orientation Index, Speed and Motility Index are presented as the average value ± the standard error of the mean (S.E.M.) of all cells. Negative Orientation Index for electrotaxis indicates cell orientation toward the cathode of the electric fields. n stands for cell number. Reproduced with permission from Royal Society of Chemistry (RSC).*

Summarizing the results of T cell migration experiments in both PDMS and glass microfluidic devices, we conclude that similar to other lymphocyte subsets from human blood as shown in the previous electrotaxis study, activated T cells undergo strong cathode-directing electrotaxis.

6.4 Discussion and conclusion

In the present study, we employed a PDMS microfluidic device and a glass microfluidic device with integrated on-chip electrodes for electrotaxis experiments. Using both devices, we successfully demonstrated the cathode-directing electrotaxis of activated T cells from human peripheral blood and the characteristics of electrotactic migration of T cells are compared with T cell chemotaxis. To our best knowledge, this is the first demonstration of activated T cell electrotaxis and the first direct comparison of electrotaxis and chemotaxis of the same cell type in the same experimental platform.

Compared to the previously reported plastic microfluidic electrotaxis device, the microfluidic devices employed in the present study improved the control of channel profile. Importantly, the PDMS device and the glass device are complementary benefiting from their own unique features. The main limitation of the PDMS device is the poor control for positioning electrodes in the medium reservoirs that may complicate the experimental conditions. Such limitation is complemented by the glass electrotaxis device that has integrated on-chip electrodes. On the other hand, the glass device requires more complicated microfabrication and is inconvenient to duplicate. Clear demonstration of the cathode-directing electrotaxis of activated T cells in the two devices enhanced the experimental accuracy. In the PDMS device, the platinum electrodes are placed in the medium reservoirs with the volume (~150 μL) much bigger than it in the microchannel (~10 μL). Therefore, the possible toxicity of the electrodes to the cells in the

channel is minimized. In the glass device, because the electrodes are integrated on the chip that crosses the channel, the toxicity issue can be more significant. However, our experiments were typically finished within 20 min and the micro-electrodes are small in size (200 μm in width and 180 nm in depth and crosses 500 μm wide channel) so we speculate that the presence of the electrodes itself did not significantly affect cell migration. Despite of the success of the current devices, the discussion above suggests the need for developing more sophisticated experimental strategies for better control of electrode products and other influencing factors such as pH changes, temperature variation and the flow caused by unbalanced medium levels in the two reservoirs.

T lymphocytes are important players for the adaptive immune system. It consists of diverse sub-populations each exhibits unique migratory and trafficking properties. Circulating T cells migrate into secondary lymphoid tissues such as lymph nodes directed by chemokines. In these tissues, T cells interact with antigen presenting cells (APCs) such as dendritic cells leading to the activated stage. T cell activation and migration are crucial for inducing the subsequent immune responses such as clonal expansion of T cells, antibody production by B cells, cytokine secretion, and other effector T cell functions. Therefore, understanding the guiding mechanism for activated T cell migration will generate important insights into the complex adaptive immunity and may enable new clinical applications for cell migration mediated problems such as autoimmune diseases. Previous study showed that most lymphocyte subsets from human blood undergo the cathode-directing electrotaxis, suggesting activated T cells may be capable of electrotactic migration as well. Indeed, our current study showed that T cells activated by anti-CD3/CD28 antibodies migrate toward the cathode of the applied DC electric fields in microfluidic devices. In the skin wound setting, such electrotactic migration in response to the wound generated electric fields

will allow activated T cells to be recruited to the wound to facilitate the wound induced immune responses. In addition, activated T cells may be electrically directed by an externally applied electric field to facilitate immune responses in a noninvasive manner and such approach may be useful for treating autoimmune diseases and for anti-cancer therapy.

In contrast to the well-studied chemotaxis mechanisms for directing immune cell migration and trafficking, the cellular mechanisms for electrotactic migration are not well defined. It is convenient to first compare electrotaxis and chemotaxis to search potential commonalities and differences between the two processes. However, so far there has been no direct comparison of the quantitative characteristics of electrotactic and chemotactic migration of the same cell type in similar experimental systems. In the present study, we analyzed electrotaxis and chemotaxis of activated T cells in PDMS microfluidic devices. Quantitative comparison showed that electrotactic migration of activated T cells exhibit comparable motility to chemotaxing T cells, and similar or even higher orientation responses comparing to T cell chemotaxis to a chemokine CCL19 gradient. These results suggest that electrotaxis of activated T cell is as effective as chemotaxis and may potentially overcome chemotactic guidance in co-existing chemoattractant gradients and electric fields. However, our current study does not exclude the possibility of electric field induced chemotaxis of cells. Further study with improved experimental methodologies will help clarify the effect of chemoattractants secretion by electrically stimulated cells and medium conditions. In-depth studies are also required to test a broader range of electric fields for inducing T cell electrotaxis and to compare with T cell chemotaxis in different gradient conditions. More importantly, more sophisticated microfluidic device that allow better controlled competing chemical concentration gradient and electric field is needed for examining how cells integrate or prioritize complex electrochemical guiding signals for trafficking and for developing

potential therapeutic applications, which motivated further research as described in the next chapter. On the other hand, the current study successfully demonstrated the use of microfluidic systems to identify and characterize electrotaxis of activated T cells.

Chapter 7

T cell migration in co-existing chemical gradient and DC electric field in microfluidic devices

7.1 Introduction

In addition to the complex mechanisms of electrotaxis itself [6, 14], an additional layer of complexity results from the co-existence of chemical fields and electric fields in tissues that can potentially cross-modify the chemical or electric field profiles. Studies toward dissecting chemotactic and electrotactic guidance for cell migration is hindered by the technical barrier of the existing electrotaxis assays that are incapable of generating independently controlled co-existing chemical gradients and electric fields.

Conventional chemotaxis assays such as transwell assays produce chemical gradients by free diffusion of chemoattractant molecules so that the gradient profiles vary over time [15-17, 19, 80]. The gradients in these assays can be further modified by electric field applications. The commonly used electrotaxis assays measure cell migration in electric fields inside a cell chamber built within a petri dish [3, 23-25, 27, 47, 81]. The dish-based electrotaxis assays are not capable of creating chemical gradients. Microfluidic devices offer the advantages in miniaturization and cellular environmental control, and various gradient-generating devices have been increasingly developed and applied to cell migration and chemotaxis research over the last decade or so [20]. More recently, the potential of microfluidic devices for electrotaxis studies of different cell types started to be realized [28]. The existing microfluidic devices basically generate controlled electric fields inside a straight microfluidic channel, but do not allow superposition with

chemical gradients. Integration of chemical gradient-generation and electric fields applications in microfluidic devices for studying interactions of these two guiding factors for cell migration is technically challenging because electric fields may modify chemical gradient profiles due to the electromigration mobility of chemoattractant molecules. On the other hand, an earlier study employing a stripe assay has demonstrated the altered chemotaxis of human blood granulocytes by an externally applied electric field [82]. In addition, our recent study comparing human blood T cell chemotaxis and electrotaxis using separate microfluidic devices suggested the differential potency of chemokine gradients and dcEF for attracting T cells. Taken together, the importance of understanding cell migration in co-existing chemical gradients and electric fields, the demonstrated alteration of cell migration in combined chemical and electric fields, and the anticipated trend of microfluidics-based research for electrotaxis strongly motivated us to explore new microfluidics-based strategies of controlling single and co-existing chemical gradients and electric fields for cell migration research.

In the present study, we developed a polydimethylsiloxane (PDMS)-based microfluidic device that integrates a flow-based gradient-generating module with electric fields applications through multiple parallel side microchannels. Such a device would in principle allow superposition of stable chemical gradients and dcEF across the width of the main microfluidic channel because the chemical gradient formation is dominated by continuous laminar flow mixing with negligible influence by dcEF. We characterized single and co-existing chemical gradients and dcEF in this device by multiphysics modeling to verify the hypothesized strategy of generating better controlled co-existing chemical and electric fields. To validate the function of this developed microfluidic device and to explore its use for studying chemotaxis and electrotaxis, we tested the migration of activated human peripheral blood T cells in single or co-existing chemokine CCL19

gradients and externally applied dcEF. Our results showed chemotaxis of T cells to single CCL19 gradients, and electrotaxis of T cells to the cathode of the applied dcEF. These results are consistent with our previous studies using separate microfluidic chemotaxis or electrotaxis devices, and thus serve as important controls for further testing of cell migration in co-existing chemical and dcEF in the new microfluidic device. Although we did not set specific anticipation for T cell migration in co-existing CCL19 gradients and dcEF in our experiments, we found that T cells show stronger migration toward the cathode of the dcEF in the presence of a competing CCL19 gradient that is interestingly consistent with our previous comparison between T cell chemotaxis and electrotaxis [33]. This observed differential strength of chemical and electrical guidance for T cell migration suggests various possible interesting scenarios for cell migration and trafficking in complex tissue environments and thus opens up new possibilities of future research.

7.2 Methodology

7.2.1 Cell preparation

Preparation of activated T cells has been described in details previously (Chapter 5.2).

7.2.2 Microfluidic device preparation

The standard fabrication method of PDMS microfluidic devices has been described in Chapter 5.1. For the device in the current study (Fig. 7-1), one outlet well (4 mm diameter holes) at the end of a 350 μm (W) × 1 cm (L) channel (the main channel), two fluid inlets (1 mm diameter holes) at the other end of the main channel, and 2 electrode wells (4 mm diameter holes) connected by the thin side channels to the main channel were punched using sharpened needles. Then the PDMS replica was plasma bonded to a glass slide. Polyethylene tubing (PE-20, Becton

Dickinson, MD) was inserted into the inlet holes to connect the microfluidic device to syringe pumps (KD Scientific, MA) with two 100 μL KD syringes containing medium or chemokine solution for fluid infusion. The main channel was connected by 20 thin channels (40 μm in width and 3 mm in length) on each side to the 2 electrode wells filled with medium, in where platinum electrodes (SPPL-010, Omega Engineering, Inc) were inserted. The electrodes were buried in a 1% agarose gel block inside the well to prevent contact of possible toxic electrode byproducts with the cell culture. The electrodes were then wired to a DC power supply for electric field application. A new microfluidic device was used for each experiment.

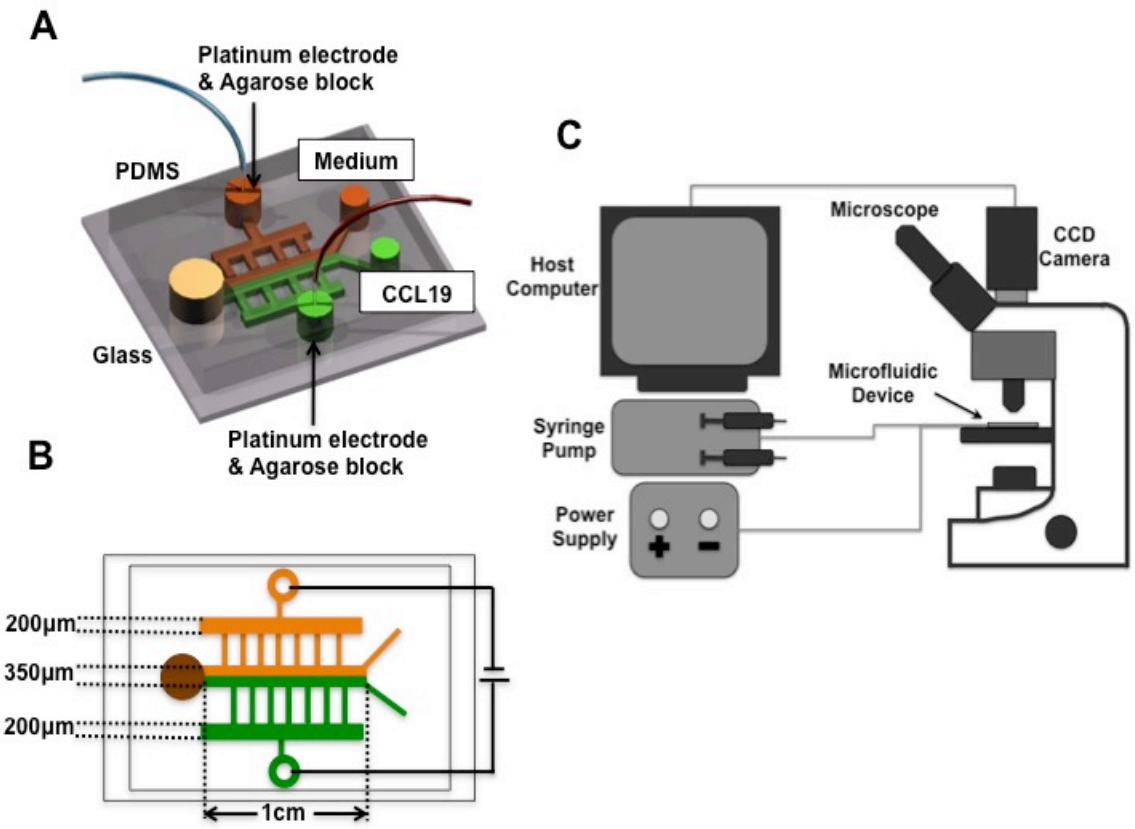

Fig 7-1. Schematic illustration of the microfluidic device. *(A) 3D schematic drawing of the PDMS microfluidic device. Green indicates CCL19 solution and orange indicates medium solution. Platinum electrodes were buried in agarose gel blocks and inserted into the electrode wells. The two electrodes were then wired to the blue (cathode) and red (anode) wires respectively that were connected to a DC power supply to apply electric fields to the device. The drawing of the side channels was simplified with symmetric configurations. (B) Top view drawing of the microfluidic device with the channel dimensions indicated. (C) Illustration of the cell migration experiment setup. Microfluidic device was placed on a microscope stage; dcEF was applied to the device through a pair of electrodes; chemokine and medium solutions were infused into the device through tubing from syringe pumps for generating chemical gradients; cell migration in the device was then recorded by time-lapse microscopy. Reproduced with*

permission from American Institute of Physics.

7.2.3 Multiphysics modeling

Multiphysics modeling and simulations were performed using COMSOL Multiphysics (v4.2) with specialized modules for modeling chemical transport and electric fields, and the parameter values were adapted from the literatures (particularly the diffusion coefficient is ~1.7×10^{-6} cm^2 /s [32] and net cationic charge value is +7 [83, 84] for chemokine CCL19).

7.2.4 Cell migration experiment setup

The microfluidic channel was coated with fibronectin (BD Biosciences, MA) for 1 hour at room temperature and blocked with 0.4% BSA for another hour before the cell migration experiment. The experimental setup is illustrated in Fig. 7-1C. Briefly, for each experiment, a few thousand cells were loaded into the microfluidic channel and allowed to settle in the fibronectin-coated channel for ~5 min. The device was maintained at 37 °C by attaching a transparent heater to the back of the coverslide (Minco, MN). The heater was powered by a DC power supply (Harrison, Canada) and was controlled by a sensorless temperature controller (Minco, MN). The temperature was calibrated to 37 °C using a digital thermometer (VWR, Canada). After the cells were settled in the channel, ~150 μL of medium (RPMI 1640 with 0.4% of BSA) was added to each well containing the agarose gel blocks and the electrodes, which are connected to a DC power supply (Central Scientific, NY) to complete the circuit. The assembled device was placed on a microscope stage (BX60, Olympus). To generate chemical concentration gradient, medium and chemokine solutions were infused into the device from the fluid inlets through tubing by syringe pumps at the total flow rate of 0.6 μL/min. The chemokine gradient was confirmed by measuring the fluorescence intensity profile of FITC-Dextran 10 kDa that has similar molecular weight of CCL19 and was added to the chemokine solution. Cell migration inside the main

channel (in the region ~7 mm downstream of the main channel) was recorded by time-lapse microscopy at 6 frames/min for at least 30 min using a CCD camera (Sensicam, Optikon). The image acquisition was controlled by NIH ImageJ (v.1.34s).

7.2.5 Data analysis

The data analysis method was illustrated in Chapter 5.4. Specially, in this study, only the cells that migrated within the relatively uniform EF region of the channel over the entire time-lapse were selected and tracked using the "Manual Tracking" plug-in in NIH ImageJ. The tracking data were exported to Excel and Origin for analysis. A custom Labview program was also used to analyze the tracking data. At least 40 cell tracks from multiple independent experiments for each condition were analyzed. Specifically, migration angles (calculated from *x*-*y* coordinates at the beginning and the end of the cell tracks) were summarized in a direction plot, which is a rose diagram showing the distribution of angles grouped in 20° intervals, with the radius of each wedge indicating the cell number.

7.3 Results

7.3.1 Generation of controlled chemical gradients and dcEF using the microfluidic device

As detailed in the Microfluidic device preparation section and illustrated in Fig. 7-1, the developed PDMS microfluidic device is a "Y" type chemical gradient-generating module with electric field applied to the main channel from the side direction through multiple thin microchannels. The fundamental principle behind this design for generating better-controlled single or co-existing chemical and electric fields is that gradient profiles will be controlled by the flows and thus minimizes the influence from the electric fields. i.e. Basically, comparing to static assays, in which electromigration of chemokine molecules will significantly modify chemokine

gradient over time, the introduction of the continuous flow in the current device limits the electromigration of chemokine molecules across the channel width as the chemokines flow through the channel length.

The use of multiple parallel channels for applying dcEF is expected to help increase the homogeneity of dcEF in the main channel. In addition, the alternating configuration of the small channels from each side of the main channel is found to help reduce small channel blocking by cells in our experiments and thus allow easier cell loading to the main channel. To verify the hypothesized functions of this design, we performed multiphysics modeling and simulations using COMSOL Multiphysics to characterize chemical gradients and electric fields in the device (Fig. 7-2).

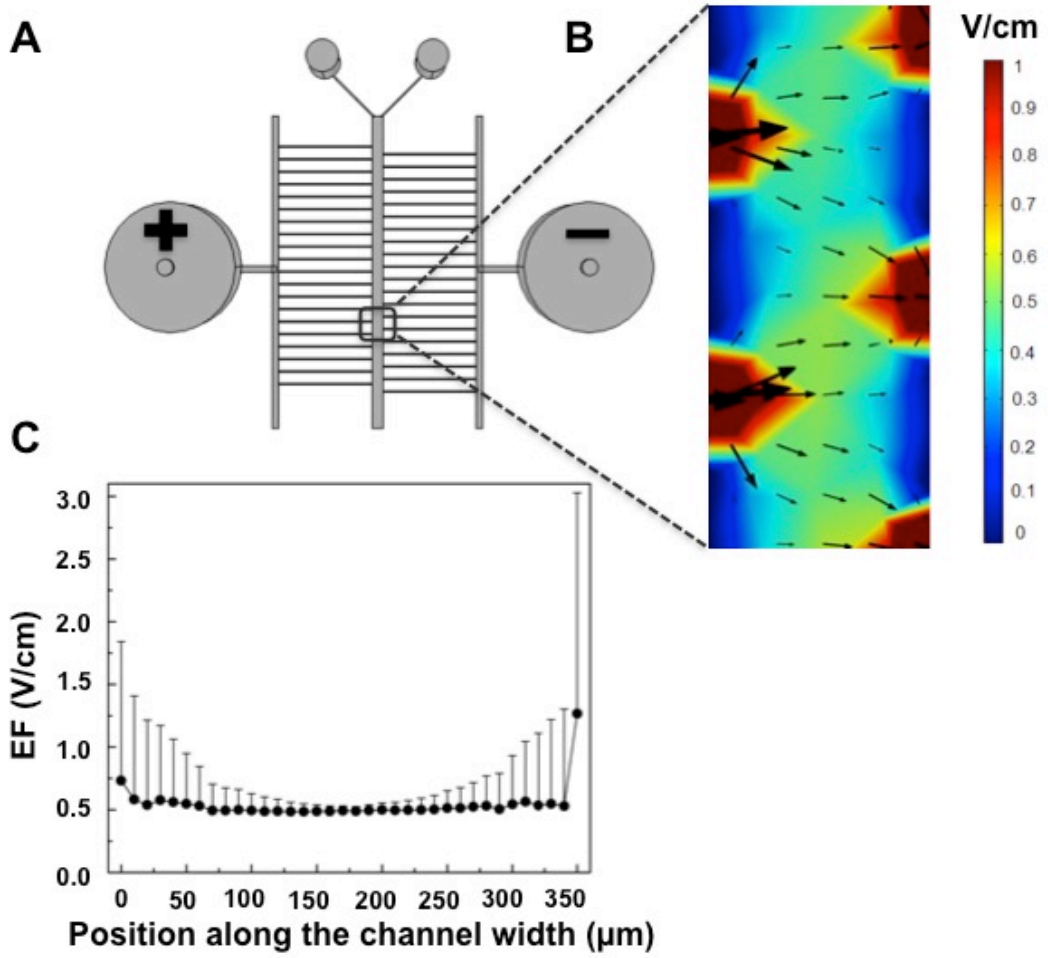

Fig 7-2. Simulation of dcEF in the microfluidic device. *(A) Top view of the microfluidic device. A 10 V of electrical potential difference was applied to the device from the two electrode wells. (B) The color map and the arrows indicate the magnitude and the direction of the dcEF in the main channel (0.75 mm (L) × 0.35 mm (W) at ~7 mm downstream of the main channel). (C) Plot of simulated dcEF across the main channel width in the region as in (B). The dcEF is presented as the average value with the error bar as the standard deviation (SD). The simulation results show that dcEF is relatively uniform in the defined center region of the main channel and its magnitude can be configured to be within the physiological strength range. Reproduced with permission from American Institute of Physics.*

First, we modeled and simulated the dcEF in the main channel of the device. As shown in our later cell migration experiments, T cells showed clear electrotaxis toward the cathode of the applied dcEF in the region ~7 mm downstream of the main channel (0.75 mm (L) × 0.35 mm (W)) when a 10 V of electrical potential difference was applied between the 2 electrode wells at the defined flow rate. Therefore, similar experimental parameters including the cell observation region, the flow rate and the applied electrical potential difference were adapted in the simulations. Our results showed that the dcEF in the center region (away from the channel edges) of the main channel is relatively uniform (Fig. 7-2) (the average EF strength is approximately 0.52 V/cm if a 10 V electrical potential difference is applied to the device). As we expected, the dcEF in the thin channels is much higher due to more significant electrical potential drop in those thin channels. In addition, the dcEF in the regions (in the main channel) where the thin channels connect the main channel is higher than the center region resulting from the boundary effect as we expected. Moreover, the dcEF varies along the 1 cm long main channel as expected. Superposition of dcEF with a 100 nM CCL19 gradient (diffusion coefficient $D = 1.7 \times 10^{-6}$ cm^2 /s; net charge of CCL19 molecule = 7) does not significantly change the dcEF or the current density in the main channel. Thus, the microfluidic device can produce a relatively uniform dcEF in the defined region of the main channel and the magnitude of the dcEF can be controlled to be within the physiological range (0.4-1.4 V/cm) [29], allowing us to analyze cell migration in defined dcEF. Therefore, as we will address in the Discussion section, the cells may exhibit different response curve to the applied electrical potential difference in the two different microfluidic devices given the different dcEF and electrical current density. Second, we modeled and simulated the chemokine gradient in the main channel of the device. We adapted similar diffusion coefficient (~1.7×10^{-6} cm^2 /s) and net cationic charge values (+7) for chemokine

CCL19 from the literatures in the simulations. Our results showed that the gradient profile in the same region of the main channel where we characterized the dcEF is maintained by the flows (total flow rate = 0.6 μL/min) and is not significantly affected by the dcEF induced electromigration of the chemokine molecules (Fig. 7-3) as shown by the F test (p = 0.82) to compare the gradient profiles with or without dcEF [85].

Taken together, modeling and simulation of the microfluidic device validated the hypothesized functions of the device for configuring better controlled single or co-existing chemical gradients and dcEF, and provided the quantitative characteristics of chemical and electric fields in the device that will guide the designs of cell migration experiments for studying chemotaxis, electrotaxis and their interactions.

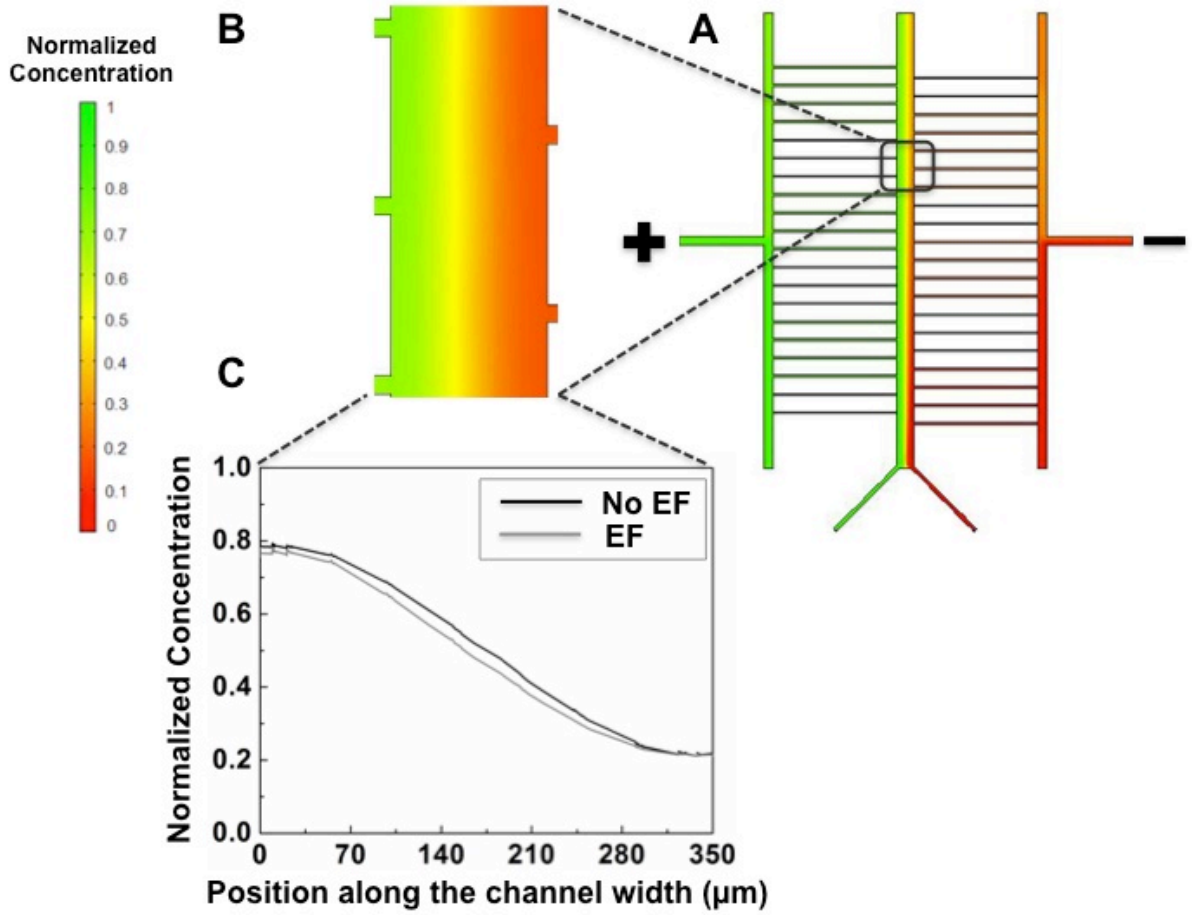

Fig 7-3. Simulation of chemical concentration gradients with dcEF application in the microfluidic device. *(A) Simulated normalized CCL19 gradient in the main channel of the microfluidic device when a 10 V electrical potential difference is applied to the device through the 2 electrode wells. (B) Enlarged view of the CCL19 gradient in the boxed region in the main channel as indicated in (A) (~7 mm downstream of the main channel). (C) Plot of simulated gradient across the main channel width in the region as in (B) with (grey) or without (black) the applied dcEF. The simulation results show that the gradient profile is not significantly affected by the applied dcEF. The p value of the F test comparing the gradient profiles is 0.82. Reproduced with permission from American Institute of Physics.*

7.3.2 T cell chemotaxis to single chemokine gradients in the microfluidic device

Using the developed microfluidic device, we experimentally analyzed the migration of activated human peripheral blood T cells in a single 100 nM CCL19 gradient. For future reference within this chapter, the cells were analyzed in the region ~7 mm downstream of the main channel for all our experiments. As we expected, T cells show chemotaxis to the CCL19 gradient (Fig. 7-4) that is consistent with previous chapter using the simple "Y" shape microfluidic device [33]. By contrast, in the uniform medium control experiment, cells migrate randomly with reduced speed (Fig. 7-4). It is worth pointing out that the exact values of these cell migration parameters vary between the current data and our previous chapter using the simple "Y" shape device, possibly due to the device design difference, changes of several experimental conditions (e.g. cell observation region), and blood donor variations. Thus, the chemotaxis experiments demonstrate the function of the developed microfluidic device for analyzing cell chemotaxis in single chemokine gradients.

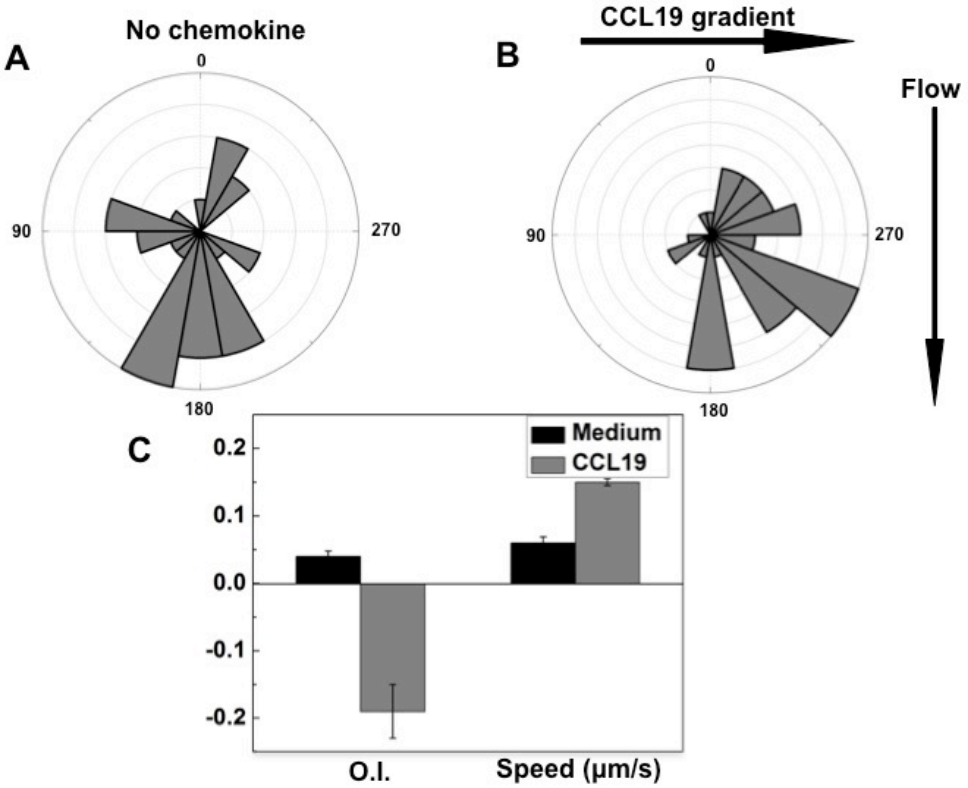

Fig 7-4. T cell chemotaxis in the microfluidic device. *Angular histograms of cell migration angles in the control condition (medium only) or in a 100 nM CCL19 gradient are showed in (A) and (B), respectively. The rose diagrams show the distribution of migration angles of all cells analyzed from multiple independent experiments for each condition. The migration angles were calculated from x-y coordinates at the beginning and the end of the cell tracks, and were grouped in 20° intervals, with the radius of each wedge indicating the cell number (i.e. the radius of each circle indicates the cell number with the increment of one). (C) Orientation Index (O.I.) and Speed of cells in the control condition or in a 100 nM CCL19 gradient. The values are presented as the average ± SEM. The results show the effectiveness of the developed microfluidic device for analyzing cell chemotaxis in single chemokine gradients. Reproduced with permission from American Institute of Physics.*

7.3.3 T cell electrotaxis to single dcEF in the microfluidic device

Next, we performed electrotaxis experiments to analyze activated human peripheral blood T cells in different applied dcEF using the microfluidic device. We applied a range of DC electrical potential difference to the device and our results identified 10 V as the most effective electrical potential difference for inducing electrotactic migration of T cells toward the cathode of the dcEF in this specific microfluidic device (Fig. 7-5). As described in the previous section of this chaptet, this electrical potential difference results in a ~0.5 V/cm dcEF in the center region of the main channel, confirming the ability of T cells to respond to the physiological strength of dcEF. The speed of the cells is higher for the intermediate electrical potential difference (7 V and 10 V) within the range of the electrical potential difference tested. Thus, the electrotaxis experiments confirm the function of the developed microfluidic device for analyzing T cell electrotaxis in single dcEF.

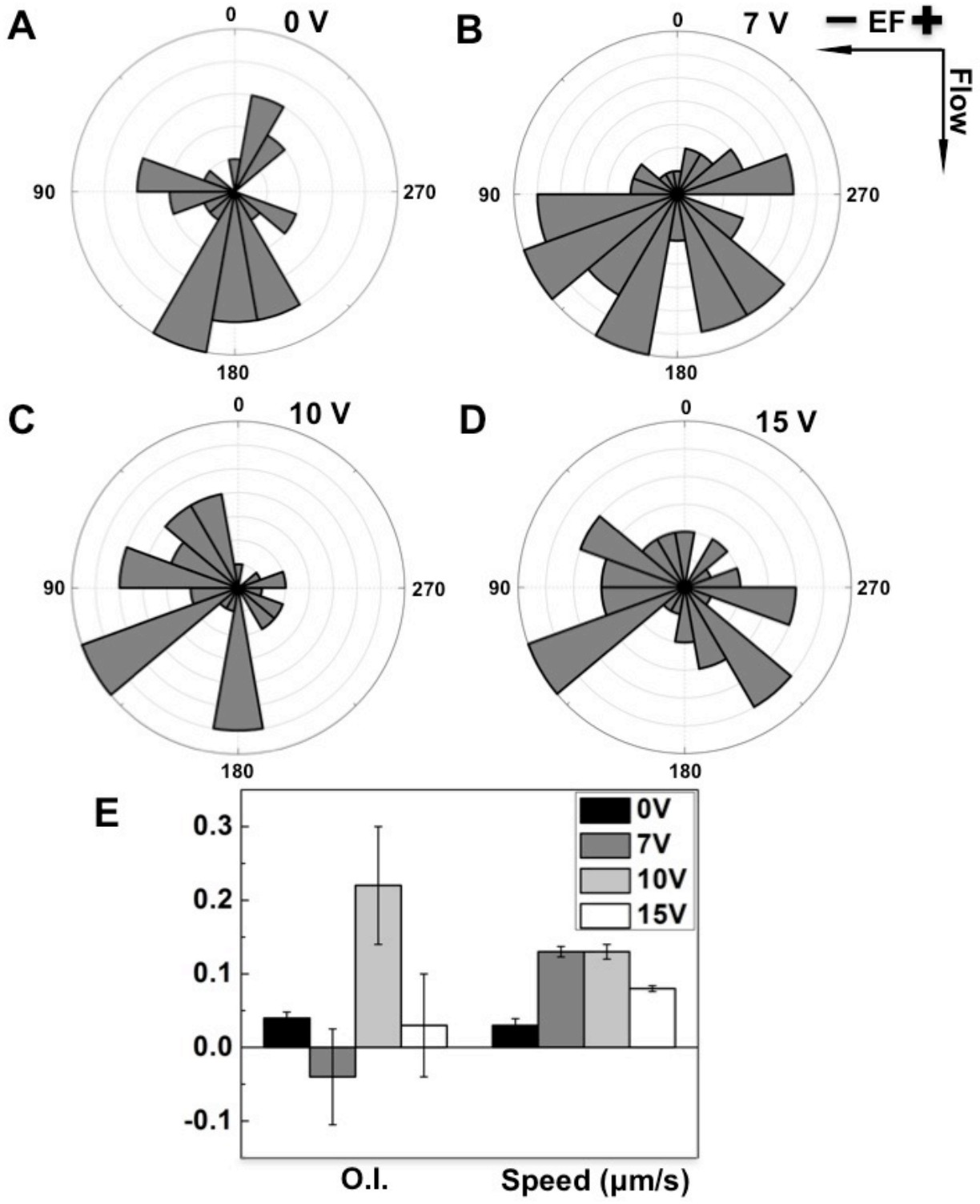

Fig 7-5. T cell electrotaxis in the microfluidic device. *(A-D) Angular histogram of cell*

migration angles in different dcEF (i.e. 0 V, 7 V, 10 V and 15 V electrical potential difference between the two electrode wells). The rose diagrams show the distribution of migration angles of all cells analyzed from multiple independent experiments for each condition. The migration angles were calculated from x-y coordinates at the beginning and the end of the cell tracks, and were grouped in 20° intervals, with the radius of each wedge indicating the cell number (i.e. the radius of each circle indicates the cell number with the increment of one). (E) Orientation Index (O.I.) and Speed of cells in different applied dcEF. The values are presented as the average ± SEM. The results show the cathode-directing electrotaxis of cells when a 10 V electrical potential difference was applied to the device, and thus demonstrate the effectiveness of the developed microfluidic device for analyzing cell electrotaxis in single dcEF. Reproduced with permission from American Institute of Physics.

7.3.4 T cell migration in competing chemokine gradient and dcEF in the microfluidic device

Based upon the separate chemotaxis and electrotaxis experiments as describe above, we further tested the migration of activated human peripheral blood T cells in co-existing CCL19 gradient and dcEF. In this experiment, we configured the CCL19 gradient (100 nM) and the dcEF (10 V across the device) along the opposite directions, creating a competing scenario between the chemokine gradient and the dcEF for directing T cell migration (Fig. 7-6). Our results show that the migration of T cells to the CCL19 gradient or to the dcEF is significantly altered compared to it in single CCL19 gradients or single dcEF. Interestingly, the net migration of T cells is toward the cathode of dcEF with reduced orientation index. The speed of T cells is not affected compared to it in single CCL19 gradient or single dcEF. These results demonstrate the function of the developed microfluidic device for analyzing T cell migration in co-existing chemical and electric fields and the altered cell migration suggests interesting interactions between chemotaxis and electrotaxis.

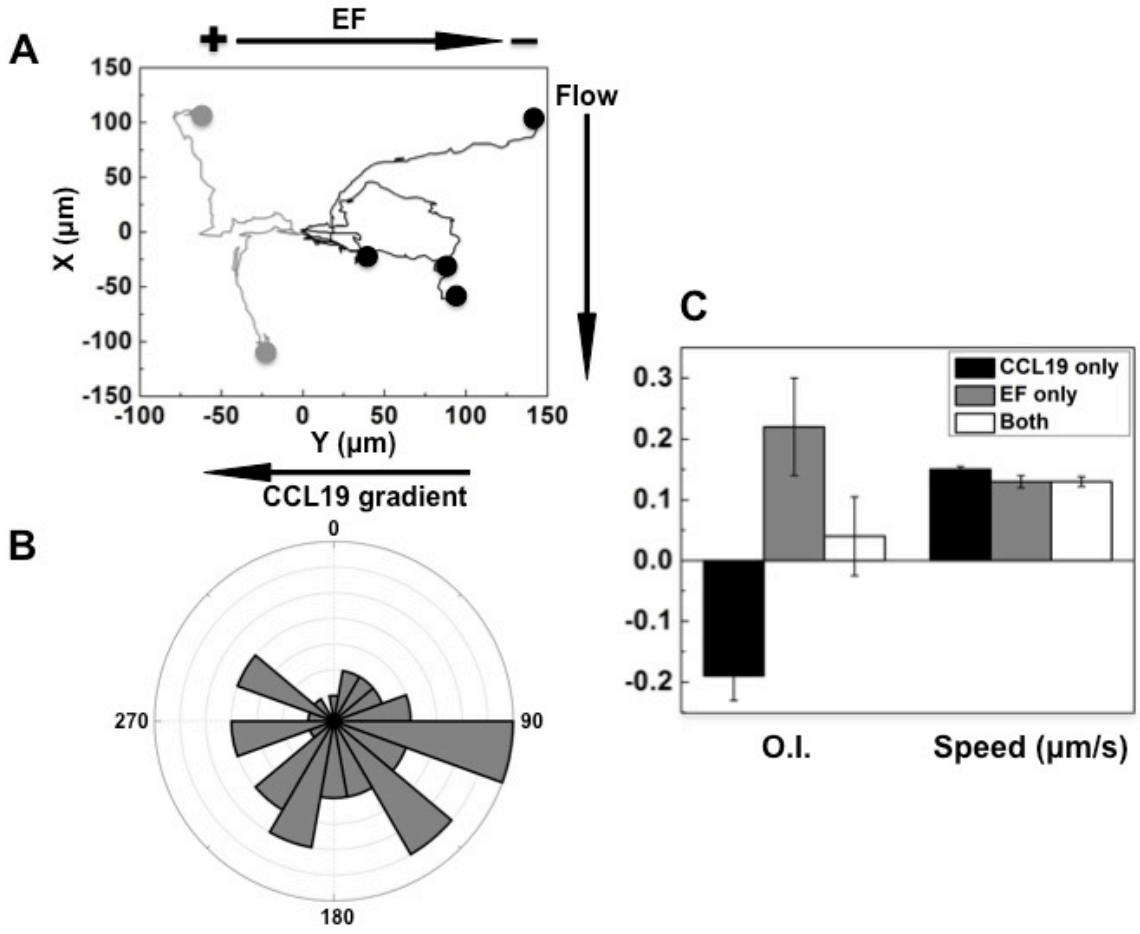

Fig 7-6. T cell migration in competing CCL19 gradients and dcEF in the microfluidic device. *(A) Migration tracks of 6 cells from a representative experiment with 2 cells (grey) migrating toward the 100 nM CCL19 gradient (left) and 4 cells (black) migrating toward the cathode of the applied dcEF (10 V across the device with the cathode on the right). (B) Angular histogram shows the distribution of migration angles of all cells analyzed from multiple independent experiments. The migration angles were calculated from x-y coordinates at the beginning and the end of the cell tracks, and were grouped in 20° intervals, with the radius of each wedge indicating the cell number (i.e. the radius of each circle indicates the cell number with the increment of one). (C) Orientation Index (O.I.) and Speed of T cells in single CCL19 gradient,*

single dcEF or competing CCL19 gradient and dcEF. The values are presented as the average ± SEM. The results show the stronger cell migration toward the cathode of the applied dcEF in the presence of a competing CCL19 gradient. Reproduced with permission from American Institute of Physics.

Altogether, our results characterized the developed microfluidic device for configuring better controlled single or co-existing chemical gradients and dcEF. The functions of the device for analyzing cell chemotaxis, electrotaxis, and cell migration in co-existing chemical gradients and electric fields were successfully demonstrated.

7.4 Discussion and conclusion

In the present study, we developed a PDMS-based microfluidic device that can generate separate chemical concentration gradients and electric fields or better controlled co-existing chemical gradients and electric fields. Such a device is critically required for analyzing cell migration in complex chemical and electrical guiding environments but it was not available previously. The T cell migration experiments using this developed device successfully demonstrated these unique functions of the device. Thus, the developed device presents advancement from the previous single function-based microfluidic chemotaxis and electrotaxis devices to an integrated device for configuring more complex but better controlled electrochemical guiding environments for cell migration analysis.

The current design of the device serves as a first step to explore the hypothesized principle for generating better-controlled single or co-existing chemical gradients and dcEF. We successfully demonstrated the effectiveness of this concept in our modeling and cell migration studies. On the other hand, the design of the microfluidic device can be further improved for better performance. For example, the thickness of the connecting thin channels can be decreased using a multi-height fabrication procedure [86], to further reduce flow disturbance and facilitate cell loading. Similarly, the connecting junctions between the thin channels and the main channel can be narrowed by increasing the fabrication resolution for the same purpose of reducing flow

disturbance and increasing the uniform dcEF region in the main channel. Furthermore, the joining channel for the thin channels on each side of the main channel can be designed to bring them to equal electrical potential (possibly by making long and big electrode wells that connect all the thin channels or by patterning on-chip electrodes across the thin channels [33]). Our preliminary modeling and simulations suggest that such a design can improve the uniformity of the dcEF along the main channel. To exclude the possible effect of electrolysis (around the electrodes) induced pH change on gradient formation and cell migration, we measured the pH in our device before and after the dcEF application. The results showed that the pH in the anode electrode well decreased and the pH in the cathode electrode well increased, confirming the expected electrolysis of medium. However, the pH value remains unchanged in the medium well for the main channel. We have confirmed this unaffected pH in the main channel at the equilibrium state by multiphysics simulation and we believe this is due to the flow in the channel. In the current study, we used FITC-Dextran 10 kDa that has similar molecular weight of CCL19 to indirectly verify the CCL19 gradient without the dcEF, and we also showed that the CCL19 gradient is similar with or without dcEF by multiphysics simulation. Ultimately, it will be important in the future to experimentally verify the chemokine gradients with or without dcEF by for instance using fluorescently-tagged chemokines (but this will require the fluorescently-tagged CCL19 without affecting its diffusivity and net charge).

A key interesting finding from the current T cell migration experiments using this developed device is that T cells show stronger migration toward the cathode of the applied dcEF in the presence of a competing CCL19 gradient (the dcEF strength and the chemokine gradient condition for inducing optimal electrotaxis or chemotaxis were chosen). This result is consistent with the comparison between chemotaxis and electrotaxis of T cells in single chemokine

gradients or dcEF using this device or as shown in our previous studies using single function microfluidic devices [33], providing the initial experimental basis for discussing potential mechanisms behind the competition of chemotaxis and electrotaxis. For example, cells respond to chemical gradients through their specific surface receptors for the chemoattractant molecules and the activated receptors trigger complex downstream chemotactic signaling cascades [87-89]. By contrast, such receptor specific signaling was not found for electrotaxis. On the other hand, it has been demonstrated that electrotaxis shares many downstream signaling processes for chemotaxis [3, 38]. Therefore, assuming chemotaxis and electrotaxis employ separate non-interacting upstream signaling mechanisms but share the downstream signaling pathways, the competition of chemotaxis and electrotaxis can be possibly viewed as a simple algebraic integration between the chemical gradient activated and the dcEF activated downstream signaling events within the same downstream signaling molecule pool (assuming it is unlimited). This will explain the observed stronger migration of T cells toward the applied dcEF over the chemokine gradient due to the stronger electrotactic attraction. In the second scenario, previous studies and our recent modeling study have suggested that dcEF may polarize various cell surface receptors by electrophoresis allowing cells to sense the dcEF and moreover to overcome chemoattractant gradient by preferentially migrate toward the dcEF [14, 90-92]. Such a unified chemoattractant receptor based picture is also consistent with our observed stronger electrotactic migration of T cells over a competing CCL19 gradient. Base on this theory, we would predict that CCR7, the receptor for CCL19, can be polarized toward the cathode of the dcEF (note that receptor polarization is a complex process that cannot be simply predicted by the receptor net charge and thus needs to be experimentally determined [91]). We would further predict that blocking CCR7 (using antibodies for example) will not only inhibit T cell chemotaxis to CCL19

or CCL21, but may also reduce T cell migration toward the dcEF in competing CCL19 gradient and dcEF. On the other hand, such a theory does not account for the observed T cell electrotaxis in single dcEF wherein no CCL19 is presented. Finally, the current cell migration data in competing CCL19 and dcEF with selected chemokine dose and dcEF strength does not exclude the possibility that the competition outcomes may vary for other combinations of chemokine gradients and dcEF and for other cell types, which will be interesting to investigate in future studies using this developed microfluidic device.

In tissues, multiple chemical concentration gradients as well as electric fields can potentially co-exist, and thus cells can be exposed to different spatiotemporal configurations of single or overlapping chemoattractant gradients and dcEF [28]. In the wound setting, both wound released chemical gradients and wound-generated dcEF can potentially attract the surrounding epithelial cells in a coordinated manner to facilitate wound healing [28]. Similarly, combined chemical gradients and dcEF may enhance immune cell recruitment or cancer metastasis based on the reported chemotaxis and electrotaxis ability of various immune cell subsets and different metastatic cancer cells [24, 29, 33, 69]. Equally importantly, there are likely situations that chemical gradients and dcEF direct cells along the opposite directions, and the competition outcomes will lead to different physiological consequences. The observed stronger electrotactic migration of cells in competing chemokine gradients and dcEF may support the possible scenario, in which cells from distant tissues are effectively recruited by dcEF to the surrounding regions of a defined target (e.g. the wound) without distraction by the surrounding tissue derived "irrelevant" chemoattractant gradients. Once the cells get closer to the final target, the target derived chemoattractant gradients and dcEF will collaborate to enhance cell recruitment to the target. In this regard, the more potent but non-specific dcEF may work more effectively for long-

range recruitment of relevant cells to the surrounding regions of the target compared to the complete chemical based multi-step cell recruitment model through multiple sequentially arrayed chemoattractant sources as proposed previously [80]. The flow conditions used in our device is not physiologically relevant to the real situations in tissues and therefore dcEF may indeed modify chemical gradients in tissues. On the other hand, in the absence of flows, one can imagine that dcEF may either weaken the competing gradient strength of chemoattractants with positive net charge (e.g. CCL19 and CCL21) or enhance these chemical gradients when they are along the dcEF direction. In those cases, cell migration toward dcEF may be further enhanced. The predictions will be different for chemoattractants with negative net change or for anode-electrotaxing cell types. Therefore, a better understanding of the relative potency, and more importantly, the competition of chemical gradients and dcEF for attracting different cell types, will help dissect the complex coordination of cell migration and trafficking in tissues in the context of different physiological and pathological processes. The developed microfluidic device will critically enable research toward this direction. Furthermore, characterizations of cell migration in competing chemoattractant gradients and dcEF may provide important scientific basis for developing new therapeutic strategies for cell trafficking mediated diseases or physiological processes such as autoimmune diseases, cancers and wound healing, by electrically manipulating cell trafficking and positioning in tissues. The observed stronger cell migration toward dcEF over chemoattractant gradients in the current study argues the possibility of such clinical applications.

In conclusion, the present study developed a novel microfluidic device that offers the ability to quantitatively analyze cell migration in better controlled single or competing chemoattractant gradients and dcEF. The developed device can be useful for a broad range of cell migration and

trafficking related research areas. Further development of the device and cell migration and trafficking studies enabled by the device will generate important insights into the complex biological mechanisms of electrotaxis and its interaction with chemotaxis with implications for physiological processes, disease pathologies as well as clinical applications.

Chapter 8

Conclusion remarks and outlook

Recent developments of microfluidic cell migration devices offers researchers significantly improved control of cellular environments and allows better quantitative investigations of the complex chemical and electrical guiding mechanisms of cell migration. In the research of this thesis, we developed and characterized several microfluidic cell migration devices and these devices were successfully used to study the migration of activated human peripheral blood T cells in chemical gradients and electric fields. In addition to demonstrating chemotaxis and electrotaxis of T cells, we for the first time compared the quantitative characteristics of T cell chemotaxis and electrotaxis using comparable microfluidic devices. Furthermore, using the microfluidic device that produces controlled co-existing chemical gradients and electric fields, we directly tested the competition of these two guiding factors in directing T cell migration and our results suggested interesting insights of how cells sense and prioritize different guiding cues. These microfluidic devices can also be useful for studying chemotaxis, electrotaxis and their interplays of other cell types.

At the technical level, although various microfluidic devices are successfully used in cell migration studies, there are still issues need be addressed before microfluidics-based approaches can be routinely used in biological and biomedical labs. Particularly, for microfluidic chemotaxis devices, there are currently no standardized materials or designs for device making. Therefore both the development and use of microfluidics devices requires background knowledge and specialized skills for the researcher to properly devise, employ, and control these complex systems. In the future, a standardized and user-friendly microfluidic platform needs to be

developed that could be applied to different experiments to study the migration and movement of different biological organisms in simple or complex chemoattractant gradients. Compared to the diverse designs of microfluidic chemotaxis devices, microfluidic electrotaxis devices including the ones reported in this thesis are similar in their design and operating principle, suggesting the potential for standardizing the format of microfluidic electrotaxis devices with flexible designs depending on the applications. To further improve the microfluidic devices developed in this thesis, we will focus on generating more uniform dcEF with superimposed chemical gradients and on developing more sophisticated microfluidic devices to allow high-throughput experimentation, flexible application of simple or complex electric fields, and sensitive detection of electrotactic responses of cells/organisms. In addition, we will further develop microfluidic electrotaxis devices in 3D environments to better mimic ECM in tissues.

For the biological aspects, although research including the T cell studies in this thesis identified the ability of different cell types for undergoing electrotaxis, more efforts are required to better understand the underlying biological mechanisms. In this regard, a much wider range of possible signaling mechanisms must be examined that require genetic approaches to manipulate the target signaling molecules/pathways and will benefit from proteomics-based and systems biology approaches. Furthermore, characterizations of electrotaxis of cells/organisms in response to complex electrical signals such as temporally varying electric fields are required. Based on the research from this thesis, we can further test the signaling mechanisms for T cell electrotaxis such as G protein signaling, PI3 kinase signaling and calcium signaling by integrating cell biology approaches and the use of the developed microfluidic devices. Furthermore, high-throughput electrotaxis devices will critically enable efficient testing of T cell migration in different combinations of chemical gradients and electric fields to better understand the

interactions between chemotaxis and electrotaxis in directing T cell migration.

References

1 Luster, A.*, et al.* (2005) Immune cell migration in inflammation: present and future therapeutic targets. *Nat Immunol* 6, 1182-1190

2 Muller, A.*, et al.* (2001) Involvement of chemokine receptors in breast cancer metastasis. *Nature* 410, 50-56

3 Zhao, M.*, et al.* (2006) Electrical signals control wound healing through phosphatidylinositol-3-OH kinase-gamma and PTEN. *Nature* 442, 457-460

4 Behar, T.*, et al.* (1994) GABA-induced chemokinesis and NGF-induced chemotaxis of embryonic spinal cord neurons. *The Journal of Neuroscience* 14, 29-38

5 Jin, T.*, et al.* (2008) Chemotaxis, chemokine receptors and human disease. *Cytokine* 44, 1-8

6 Zhao, M. (2009) Electrical fields in wound healing-An overriding signal that directs cell migration. *Semin Cell Dev Biol* 20, 674-682

7 Campbell, J. and Butcher, E. (2000) Chemokines in tissue-specific and microenvironment-specific lymphocyte homing. *Curr Opin Immunol* 12, 336-341

8 Baggiolini, M. (1998) Chemokines and leukocyte traffic. *Nature* 392, 565-568

9 Yonekawa, K. and Harlan, J.M. (2005) Targeting leukocyte integrins in human diseases. *Journal of Leukocyte Biology* 77, 129-140

10 Vicente-Manzanares, M.*, et al.* (2005) Cell migration at a glance. *J Cell Sci* 118, 4917-4919

11 Berzat, A. and Hall, A. (2010) Cellular responses to extracellular guidance cues. *EMBO J* 29, 2734-2745

12 Raman, D.*, et al.* (2007) Role of chemokines in tumor growth. *Cancer Letters* 256, 137-165

13 Beeh, K.M.*, et al.* (2003) Neutrophil Chemotactic Activity of Sputum From Patients With

COPD*. *Chest* 123, 1240-1247

14 McCaig, C.*, et al.* (2005) Controlling cell behavior electrically: current views and future potential. *Physiol Rev* 85, 943-978

15 Boyden, S. (1962) The chemotactic effect of mixtures of antibody and antigen on polymorphonuclear leucocytes. *J Exp Med* 115, 453-466

16 Zigmond, S. (1977) Ability of polymorphonuclear leukocytes to orient in gradients of chemotactic factors. *J Cell Biol* 75, 606-616

17 Lohof, A.*, et al.* (1992) Asymmetric modulation of cytosolic cAMP activity induces growth cone turning. *J. Neurosci.* 12, 1253-1261

18 Zicha, D.*, et al.* (1997) Analyzing Chemotaxis Using the Dunn Direct-Viewing Chamber. pp. 449-457

19 Nelson, R.D.*, et al.* (1975) Chemotaxis Under Agarose: A New and Simple Method for Measuring Chemotaxis and Spontaneous Migration of Human Polymorphonuclear Leukocytes and Monocytes. *J Immunol* 115, 1650-1656

20 Kim, S.*, et al.* (2010) Biological applications of microfluidic gradient devices. *Integrative Biology* 2, 584-603

21 Irimia, D. (2010) Microfluidic Technologies for Temporal Perturbations of Chemotaxis. *Annual Review of Biomedical Engineering* 12, 259-284

22 Li Jeon, N.*, et al.* (2002) Neutrophil chemotaxis in linear and complex gradients of interleukin-8 formed in a microfabricated device. *Nat Biotech* 20, 826-830

23 Sato, M.J.*, et al.* (2007) Input-output relationship in galvanotactic response of Dictyostelium cells. *Biosystems* 88, 261-272

24 Djamgoz MBA*, et al.* (2001) Directional movement of rat prostate cancer cells in direct-

current electric field: involvement of voltagegated Na+ channel activity. *J Cell Sci* 114, 2697-2705

25 Song, B.*, et al.* (2007) Application of direct current electric fields to cells and tissues in vitro and modulation of wound electric field in vivo. *Nat Protoc* 2, 1479-1489

26 Gamboa, O.L.*, et al.* (2010) Electrical estimulation of retinal pigment epithelial cells. *Exp Eye Res* 91, 195-204

27 Hammerick, K.E.*, et al.* (2010) In vitro effects of direct current electric fields on adipose-derived stromal cells. *Biochemical and Biophysical Research Communications* 397, 12-17

28 Li, J. and Lin, F. (2011) Microfluidic devices for studying chemotaxis and electrotaxis. *Trends in Cell Biology* 21, 489-497

29 Lin, F.*, et al.* (2008) Lymphocyte electrotaxis in vitro and in vivo. *J Immunol* 181, 2465-2471

30 Minc, N. and Chang, F. (2010) Electrical Control of Cell Polarization in the Fission Yeast Schizosaccharomyces pombe. *Current Biology* 20, 710-716

31 Rezai, P.*, et al.* (2010) Electrotaxis of Caenorhabditis elegans in a microfluidic environment. *Lab Chip* 10, 220-226

32 Lin, F. and Butcher, E. (2006) T cell chemotaxis in a simple microfluidic device. *Lab Chip* 6, 1462-1469

33 Li, J.*, et al.* (2011) Activated T lymphocytes migrate toward the cathode of DC electric fields in microfluidic devices. *Lab on a Chip* 11, 1298-1304

34 Fletcher, D.A. and Theriot, J.A. (2004) An introduction to cell motility for the physical scientist. *Phys Biol* 1, T1-10

35 Ridley, A.J.*, et al.* (2003) Cell migration: integrating signals from front to back. *Science* 302, 1704-1709

36 Kunkel, E.J. and Butcher, E.C. (2003) Plasma-cell homing. *Nat Rev Immunol* 3, 822-829

37 Kunkel, E. and Butcher, E. (2002) Chemokines and the tissue-specific migration of lymphocytes. *Immunity* 16, 1-4

38 Zhao, M. (2007) PTEN: a promising pharmacological target to enhance epithelial wound healing. *British Journal of Pharmacology* 152, 1141-1144

39 Lai, J.P.*, et al.* (2007) Phosphatase and tensin homologue deleted on chromosome ten (PTEN) as a molecular target in lung epithelial wound repair. *British Journal of Pharmacology* 152, 1172-1184

40 Wojtalla, A. and Arcaro, A. (2011) Targeting phosphoinositide 3-kinase signalling in lung cancer. *Critical Reviews in Oncology/Hematology* 80, 278-290

41 Funamoto, S.*, et al.* (2002) Spatial and Temporal Regulation of 3-Phosphoinositides by PI 3-Kinase and PTEN Mediates Chemotaxis. *Cell* 109, 611-623

42 Meng, X.*, et al.* (2011) PI3K mediated electrotaxis of embryonic and adult neural progenitor cells in the presence of growth factors. *Experimental Neurology* 227, 210-217

43 Mycielska, M. and Djamgoz, M. (2004) Cellular mechanisms of direct-current electric field effects: galvanotaxis and metastatic disease. *J Cell Sci* 117, 1631-1639

44 Trollinger, D.R.*, et al.* (2002) Calcium channel blockers inhibit galvanotaxis in human keratinocytes. *Journal of Cellular Physiology* 193, 1-9

45 Shanley, L.*, et al.* (2006) Influx of extracellular Ca2+ is necessary for electrotaxis in Dictyostelium. *J Cell Sci* 119, 4741-4748

46 Franke, K. and Gruler, H. (1990) Galvanotaxis of human granulocytes: electric field jump studies. *European Biophysics Journal* 18, 334-346

47 Sato, M.*, et al.* (2009) Switching direction in electric-signal-induced cell migration by cyclic

guanosine monophosphate and phosphatidylinositol signaling. *Proc Natl Acad Sci U S A* 106, 6667-6672

48 Toetsch, S.*, et al.* (2009) The evolution of chemotaxis assays from static models to physiologically relevant platforms. *Integrative Biology* 1

49 Lin, F. (2009) Chapter 15 A Microfluidics[hyphen (true graphic)]Based Method for Analyzing Leukocyte Migration to Chemoattractant Gradients. In *Methods in Enzymology* (Tracy, M.H. and Damon, J.H., eds), pp. 333-347, Academic Press

50 Lin, F.*, et al.* (2004) Generation of dynamic temporal and spatial concentration gradients using microfluidic devices. *Lab on a Chip* 4, 164-167

51 Irimia, D.*, et al.* (2006) Microfluidic system for measuring neutrophil migratory responses to fast switches of chemical gradients. *Lab on a Chip* 6, 191-198

52 Lin, F.*, et al.* (2005) Neutrophil Migration in Opposing Chemoattractant Gradients Using Microfluidic Chemotaxis Devices. *Annals of Biomedical Engineering* 33, 475-482

53 Englert, D.L.*, et al.* (2010) Investigation of bacterial chemotaxis in flow-based microfluidic devices. *Nat. Protocols* 5, 864-872

54 Saadi, W.*, et al.* (2006) A parallel-gradient microfluidic chamber for quantitative analysis of breast cancer cell chemotaxis. *Biomed Microdevices* 8, 109-118

55 Ricart, B.G.*, et al.* (2011) Dendritic Cells Distinguish Individual Chemokine Signals through CCR7 and CXCR4. *The Journal of Immunology* 186, 53-61

56 Chung, S.*, et al.* (2009) Cell migration into scaffolds under co-culture conditions in a microfluidic platform. *Lab on a Chip* 9, 269-275

57 Chen, Z.*, et al.* (2010) In Vitro Model on Glass Surfaces for Complex Interactions between Different Types of Cells. *Langmuir* 26, 17790-17794

58 Abhyankar, V.V.*, et al.* (2006) Characterization of a membrane-based gradient generator for use in cell-signaling studies. *Lab on a Chip* 6, 389-393

59 Chung, B.*, et al.* (2006) A microfluidic multi-injector for gradient generation. *Lab Chip* 6, 764-768

60 Huang, C.P.*, et al.* (2009) Engineering microscale cellular niches for three-dimensional multicellular co-cultures. *Lab on a Chip* 9, 1740-1748

61 Ambravaneswaran, V.*, et al.* (2010) Directional decisions during neutrophil chemotaxis inside bifurcating channels. *Integrative Biology* 2, 639-647

62 Robinson, K. and Messerli, M. (2003) Left/right, up/down: the role of endogenous electrical fields as directional signals in development, repair and invasion. *Bioessays* 25, 759-766

63 Nuccitelli, R. (1988) Physiological Electric Fields can Influence Cell Motility, Growth, and Polarity. In *Advances in Molecular and Cell Biology* (Kenneth, R.M., ed), pp. 213-233, Elsevier

64 Hotary, K.B. and Robinson, K.R. (1990) Endogenous electrical currents and the resultant voltage gradients in the chick embryo. *Developmental Biology* 140, 149-160

65 Hotary, K.B. and Robinson, K.R. (1994) Endogenous Electrical Currents and Voltage Gradients in Xenopus Embryos and the Consequences of Their Disruption. *Developmental Biology* 166, 789-800

66 Wang, E.-t. and Zhao, M. (2010) Regulation of tissue repair and regeneration by electric fields. *Chinese Journal of Traumatology (English Edition)* 13, 55-61

67 Yao, L.*, et al.* (2009) Electrical signals polarize neuronal organelles, direct neuron migration, and orient cell division. *Hippocampus* 19, 855-868

68 Song, B.*, et al.* (2004) Nerve regeneration and wound healing are stimulated and directed by an endogenous electrical field in vivo. *J Cell Sci* 117, 4681-4690

69 Huang, C.*, et al.* (2009) Electrotaxis of lung cancer cells in a multiple-electric-field chip. *Biosens Bioelectron* 24, 3510-3516

70 Guo, A.*, et al.* (2010) Effects of Physiological Electric Fields on Migration of Human Dermal Fibroblasts. *J Invest Dermatol* 130, 2320-2327

71 Li, X. and Kolega, J. (2002) Effects of direct current electric fields on cell migration and actin filament distribution in bovine vascular endothelial cells. *J Vasc Res* 39, 391-404

72 Pu, J. and Zhao, M. (2005) Golgi polarization in a strong electric field. *J Cell Sci* 118, 1117-1128

73 Wang, C.-C.*, et al.* (2011) Asymmetric cancer-cell filopodium growth induced by electric-fields in a microfluidic culture chip. *Lab on a Chip* 11, 695-699

74 Yan, X.*, et al.* (2009) Lung cancer A549 cells migrate directionally in DC electric fields with polarized and activated EGFRs. *Bioelectromagnetics* 30, 29 - 35

75 FÈlix, M.-A. and Braendle, C. (2010) The natural history of Caenorhabditis elegans. *Current Biology* 20, R965-R969

76 Maniere, X.*, et al.* (2011) Running Worms: C. elegans Self-Sorting by Electrotaxis. *PLoS ONE* 6, e16637

77 Paliwal, S.*, et al.* (2007) MAPK-mediated bimodal gene expression and adaptive gradient sensing in yeast. *Nature* 446, 46-51

78 Moore, T.I.*, et al.* (2008) Robust Spatial Sensing of Mating Pheromone Gradients by Yeast Cells. *PLoS ONE* 3, e3865

79 Qin, D.*, et al.* (2010) Soft lithography for micro- and nanoscale patterning. *Nat. Protocols* 5, 491-502

80 Foxman, E.F.*, et al.* (1997) Multistep Navigation and the Combinatorial Control of Leukocyte

Chemotaxis. *The Journal of Cell Biology* 139, 1349-1360

81 Tai, G.*, et al.* (2009) Electrotaxis and wound healing: experimental methods to study electric fields as a directional signal for cell migration. *Methods Mol Biol* 571, 77-97

82 Aly, A.A.*, et al.* (2008) Effects of 900-MHz radio frequencies on the chemotaxis of human neutrophils in vitro. *IEEE Trans Biomed Eng* 55, 795-797

83 Hori, Y.*, et al.* (2008) Injectable dendritic cell-carrying alginate gels for immunization and immunotherapy. *Biomaterials* 29, 3671-3682

84 Christopherson, K.W.*, et al.* (2002) Low-Molecular-Weight Heparins Inhibit CCL21-Induced T Cell Adhesion and Migration. *Journal of Pharmacology and Experimental Therapeutics* 302, 290-295

85 Lomax, R.G. (2007) *Statistical Concepts: A Second Course*.

86 Taylor, A.M.*, et al.* (2005) A microfluidic culture platform for CNS axonal injury, regeneration and transport. *Nat Meth* 2, 599-605

87 Friedl, P. and Weigelin, B. (2008) Interstitial leukocyte migration and immune function. *Nat Immunol* 9, 960-969

88 Förster, R.*, et al.* (2008) CCR7 and its ligands: balancing immunity and tolerance. *Nat Rev Immunol* 8, 362-371

89 Legler, D.F.*, et al.* (2006) Prostaglandin E2 Is Generally Required for Human Dendritic Cell Migration and Exerts Its Effect via EP2 and EP4 Receptors. *The Journal of Immunology* 176, 966-973

90 Wu, D. and Lin, F. (2011) A receptor-electromigration-based model for cellular electrotactic sensing and migration. *Biochemical and Biophysical Research Communications* 411, 695-701

91 Poo, M.-M. and Robinson, K.R. (1977) Electrophoresis of concanavalin A receptors along

embryonic muscle cell membrane. *Nature* 265, 602-605

92 Zhao, M., *et al.* (2004) Electrical stimulation directly induces pre-angiogenic responses in vascular endothelial cells by signaling through VEGF receptors. *J Cell Sci* 117, 397-405

Publications

Journal Publications

1. **J. Li**, S. Nandagopal, D. Wu, S.F. Romanuik, K. Paul, D.J. Thomson and F. Lin, "Activated T Lymphocytes Migrate Toward the Cathode of DC Electric Fields in Microfluidic Devices", ***Lab on a Chip***, 2011, 11(7), 1298 -1304.

2. **J. Li** and F. Lin, "Microfluidic Devices for Studying Chemotaxis and Electrotaxis", ***Trends in Cell Biology***, 2011, Vol. 21, 489-497.

3. **J. Li,** L. Zhu, M. Zhang and F. Lin, "Microfluidic Device for Studying Cell Migration in Single or Co-Existing Chemical Gradients and Electric Fields", ***Biomicrofluidics***, 2012, 6, 024121.

My thesis content is based on these three articles (permissions from the publishers for including these works in my thesis were obtained).

Conference Presentations

1. **J. Li**, S. Nandagopal, D. Wu, S.F. Romanuik, K. Paul, D.J. Thomson and F. Lin, "Activated T Lymphocytes Migrate Toward the Cathode of DC Electric Fields in Microfluidic Devices", *Prairie Infectious Immunology Network (PIIN) Meeting,* Russell, MB, Jun. 2011.

2. **J. Li**, S. Nandagopal, D. Wu, S.F. Romanuik, K. Paul, D.J. Thomson and F. Lin, "Activated T Lymphocytes Migrate Toward the Cathode of DC Electric Fields in Microfluidic Devices", *Manitoba Student Health Research Poster Competition*, Winnipeg, MB, Jun. 2011.

3. **J. Li**, S. Nandagopal, D. Wu and F. Lin, "Analyzing Directional Leukocyte Migration Using Microfluidic Devices", *The Manitoba Materials Conferenc*e, Winnipeg, MB, May 2011.

4. **J. Li,** S. Nandagopal, D. Wu and F. Lin, "Development of Microfluidic Devices for Studying Immune Cell Migration", *Prairie Infectious Immunology Network (PIIN) Meeting,* Saskatoon, SK, Jun. 2010.

5. **J. Li,** S. Nandagopal, D. Wu and F. Lin, "Development of Microfluidic Devices for Studying Immune Cell Migration", *Canadian Association of Physicists Congress*, Toronto, ON, Jun. 2010.